



Published in final edited form as:

Nat Neurosci. 2017 January ; 20(1): 62–71. doi:10.1038/nn.4436.

Parallel processing by cortical inhibition enables context-dependent behavior

Kishore V. Kuchibhotla^{1,2}, Jonathan V. Gill^{1,2}, Grace W. Lindsay³, Eleni S. Papadoyannis^{1,2}, Rachel E. Field^{1,2}, Tom A. Hindmarsh Sten^{1,2}, Kenneth D. Miller³, and Robert C. Froemke^{1,2,*}

¹Skirball Institute, Neuroscience Institute, Departments of Otolaryngology, Neuroscience and Physiology, New York University School of Medicine, New York, NY, 10016, USA

²Center for Neural Science, New York University, New York, NY, 10003, USA

³Center for Theoretical Neuroscience, Department of Neuroscience, Swartz Program in Theoretical Neuroscience, Kavli Institute for Brain Science, Columbia University, New York, NY 10032, USA

Abstract

Physical features of sensory stimuli are fixed, but sensory perception is context-dependent. The precise mechanisms that govern contextual modulation remain unknown. Here, we trained mice to switch between two contexts: passively listening to pure tones vs. performing a recognition task for the same stimuli. Two-photon imaging showed that many excitatory neurons in auditory cortex were suppressed, while some cells became more active during behavior. Whole-cell recordings showed that excitatory inputs were only modestly affected by context, but inhibition was more sensitive, with PV, SOM+, and VIP+ interneurons balancing inhibition/disinhibition within the network. Cholinergic modulation was involved in context-switching, with cholinergic axons increasing activity during behavior and directly depolarizing inhibitory cells. Network modeling captured these findings, but only when modulation coincidentally drove all three interneuron subtypes, ruling out either inhibition or disinhibition alone as sole mechanism for active engagement. Parallel processing of cholinergic modulation by cortical interneurons therefore enables context-dependent behavior.

Users may view, print, copy, and download text and data-mine the content in such documents, for the purposes of academic research, subject always to the full Conditions of use: http://www.nature.com/authors/editorial_policies/license.html#terms

*Correspondence to: robert.froemke@med.nyu.edu.

ACCESSION CODES

Not applicable

AUTHOR CONTRIBUTIONS

K.V.K. and R.C.F. designed experiments and wrote the manuscript. K.V.K., J.V.G., R.E.F. and E.S.P. conducted experiments. K.V.K., T.A.H.S. and J.V.G. performed analysis. G.W.L. and K.D.M. performed network modelling.

COMPETING FINANCIAL INTERESTS

The authors have no competing financial interests.

DATA AVAILABILITY STATEMENT

All code related to the modeling work is available at <http://froemkelab.med.nyu.edu/>. The data that support the findings of this study are available from the corresponding author upon request.

INTRODUCTION

Sensory stimuli convey critical information about various types of opportunities and threats, including access to nourishment, the presence of predators, or the needs of infants. The same sensory stimulus, however, can have different meanings based on previous learned associations and the contexts within which it is presented^{1–9}. For example, in language processing, the same words often have multiple meanings. Humans determine the meaning of these words by integrating prior knowledge with context to converge on a relevant interpretation^{10,11}. How does the brain enable such interpretation of sensory cues based on behavioral context? We propose that three network features would enable context-dependent processing of external stimuli by neural circuits: some components must be stable and provide a high fidelity representation of a sensory stimulus independent of context, other components must be dynamic and rapidly adjust when context changes, and finally there must be instructive signals that convey the global contextual milieu.

The mammalian auditory cortex is a major site of contextual modulation during acoustic behaviors, such that task engagement alters the spiking of principal neurons even when there is no change in the external sensory cue^{1–4,12–18}. Whether or not a stimulus will produce one or more action potentials depends on the strength and timing of excitatory and inhibitory synaptic inputs. In the adult, excitatory and inhibitory inputs are correlated during passive presentation of acoustic stimuli; this co-tuning and correlation of synaptic responses is referred to as ‘excitatory-inhibitory balance’^{19–24}. However, episodes of learning and periods of heightened attention or arousal activate neuromodulatory systems that can lead to the transient uncoupling of excitation from inhibition. This temporary period of increased excitability is effective at inducing long-term modifications of synaptic strength and receptive field organization^{25–27}. For example, pairing stimulation of the cholinergic nucleus basalis with presentation of an acoustic stimulus leads to long-term changes in receptive field properties of auditory cortical neurons^{28,29}, via changes in inhibition²⁵. Cholinergic activity also contributes to task performance by signaling positive and negative reinforcement, potentially through cortical interneurons^{6,30–32}. These links between neuromodulation, inhibitory synaptic transmission, and behavioral changes may be a general feature of nervous system organization. For example, a recent study showed that cholinergic activation of dendritic inhibition in the hippocampus can enable fear learning³³.

Context-dependent activity, however, requires rapid changes on a trial-to-trial basis. Neuronal ensembles must adjust their firing rate in a reversible manner based solely on contextual cues^{2,4,13,15}. These types of context-dependent responses diverge from the longer-term memory traces and reinforcement mechanisms that have been previously described^{6,25,30,33} but may co-opt some of the underlying circuitry. The relationship between excitation and inhibition may simply scale (up or down) based on attentional demands. However, such co-tuned scaling might restrict state-dependent flexibility. Instead, theoretical work suggests that inhibitory inputs can be preferentially regulated by neuromodulation³⁴. These synaptic and circuit mechanisms have been difficult to resolve because of the need to monitor complex input-output dynamics of excitatory, inhibitory and neuromodulatory inputs. Here we take an integrative approach to measure, manipulate and model the impact of behavioral engagement on a cortical circuit in behaving mice. We combine (i) cell-type

specific two-photon calcium imaging to measure network output, (ii) whole-cell voltage-clamp recordings of excitatory and inhibitory inputs, (iii) calcium imaging of cholinergic axons to monitor neuromodulatory inputs, (iv) optogenetics to manipulate all core components of the circuit, and (v) a theoretical model to integrate and test the robustness of our findings.

RESULTS

A context-switching task that depends on the auditory cortex

To determine how behavioral context influence network dynamics, we trained head-fixed mice on an active versus passive context-switching task using a block-based experimental design (Fig. 1a, Supplementary Figure 1a). For the active listening context (“active context”), we trained animals on an auditory go/no-go stimulus recognition task. Mice learned to lick for a water reward provided through a lick tube after hearing the reinforced conditioned stimulus (the target tone, Supplementary Figure 1b) and to withhold from licking after hearing an unrewarded pure tone of a different frequency (the foil tone, Supplementary Figure 1c). In the passive context, the lick tube was removed and mice were exposed to the same sounds (target and foil) but animals did not produce a behavioral response (Supplementary Video 1). Importantly, the absence of licking in the passive context (i.e., the sensorimotor response in response to the target tone) was completely voluntary since it was not reinforced with reward or punishment. The choice to behave was therefore externally triggered by the presence or absence of the lick tube. This task required auditory cortex, as bilateral muscimol infusions into auditory cortex significantly impaired behavioral performance in the active context (Fig. 1b; $n=3$ animals, $d'=3.0\pm 0.2$, muscimol $d'=0.8\pm 0.3\%$, mean \pm s.e.m., $p<0.05$, Student’s paired two-tailed t-test).

Rapid and reversible context-dependent changes in A1 network output

To determine how auditory cortex responds to the conditioned stimuli in both contexts, we first imaged the activity of 1,595 neurons in cortical layer 2/3 in five mice in the two different contexts. To select the target and foil tones, we performed two-photon imaging in awake mice virally expressing GCaMP6s while presenting pure tones between 4–64 kHz at 70 dB sound pressure level (SPL) before behavioral training (Fig. 1c, d). We used two criteria in selecting the stimuli: 1) the imaged focal planes had neurons with tone-evoked calcium responses to the target and foil (Fig. 1c), and 2) both tones were within one octave of each other (Fig. 1d). After selecting the target and foil, we conducted behavioral training (Fig. 1e, Supplementary Figure 1d) until mice reliably responded to the target tone with licking (hits) and withheld licking responses to the foil tone (correct rejects) (Fig. 1e, $n=23$ mice, $d'=2.5\pm 0.3$, hit rate= $92.5\pm 1.7\%$, mean \pm s.e.m.). All mice reached threshold within 3–13 sessions (Supplementary Figure 1d). All imaging data underwent a detailed motion-correction protocol (see Experimental Procedures, Supplementary Figures 2–3, Supplementary Videos 2–3) and were similar to established methods³³.

We observed broad-based suppression of neural responses to both the target and foil tones during the active context in a majority of neurons we imaged (Fig. 2a–d, $n=135/227$ target-responsive cells, $n=146/210$ foil-responsive cells, neurons were tested for responsiveness by

comparing tone-evoked response to baseline values, $p < 0.05$, Student's paired two-tailed t-test), consistent with previous extracellular recordings^{1,2,9}. Surprisingly, some neurons showed an increase in activity during the task when compared to the responses in the passive context (Fig. 2b–d, $n = 92/227$ target-responsive cells, $n = 64/210$ foil-responsive cells, $p < 0.05$ for responsiveness per neuron, Student's paired two-tailed t-test). A continuum of context-dependent changes, from suppression to facilitation, was clear across animals (Fig. 2e; $p < 0.001$, Kolmogorov-Smirnov test). The continuum from broad suppression to selective facilitation was also apparent when we restricted GCaMP6s expression to excitatory neurons (Fig. 2f–h; $n = 620$ neurons, $n = 142$ responsive, 67% suppressed, 33% activated in the active context).

Neurons responsive to either the target or foil tones showed a similar modulation by behavioral context (median context modulation for target tones: $-13.8 \pm 4.8\%$, median context modulation for foils: $-16.8 \pm 4.0\%$, median $\pm 95\%$ confidence intervals, Fig. 2c, d, bottom; dashed lines denote significance threshold generated from a shuffled dataset). This indicates that task-related modulation was not due to expectation of reward on a given trial or delivery of water. Changes in neural activity occurred rapidly, within 1–2 trials of switching contexts (Supplementary Figure 4), supporting the existence of an ensemble-level switch. Neurons whose best frequency was close to either the target or foil (best frequency < 0.25 octaves from target or foil; target, $n = 51$ cells, foil, $n = 24$ cells) were most likely to be suppressed during the active context (Supplementary Figure 5). Conversely, neurons with best frequencies that were further from the target or foil (best frequency > 0.25 octaves from target and foil) were more likely to be more responsive during the active context (Supplementary Figure 5). Thus, behavioral context rapidly alters A1 responses, leading to a continuum of response suppression and facilitation.

Cell-type specific activity profiles in auditory cortex

The activity of diverse inhibitory subpopulations may play a key role in generating the network output phenotype of both suppression and facilitation. We focused on the three interneuron subtypes that make up $\sim 80\%$ of cortical interneurons: PV-positive, SOM-positive, and VIP-positive interneurons³⁵. These three interneuron subtypes are thought to make up a canonical cortical circuit^{7,31,36}. To examine the responses of inhibitory cells, we expressed GCaMP6s in *PV-tdTomato*, *SOM-tdTomato* or *VIP-tdTomato* mice and imaged 65 PV+, 159 SOM+ and 90 VIP+ layer 2/3 interneurons in A1 during active and passive contexts (Fig. 3; cell inclusion approach in Supplementary Figure 6). In contrast to the excitatory pool (Fig. 3b), inhibitory neurons showed robust change in baseline activity, with VIP+ interneurons showing the largest changes, followed by SOM+ interneurons and then PV+ interneurons (Fig. 3b). Tone-evoked responses were also modulated in all subtypes with PV+ and SOM+ interneurons (Fig. 3c–f) preferring the active context unlike the excitatory pool (Fig. 3c–d; 'PV+', $n = 31$ tone-responsive PV+ interneurons, 19/31 increased activity, $p < 0.01$ compared to excitatory pool where 47/142 increased activity, Fisher's exact test; Fig. 3e–f, 'SOM+', $n = 20$ tone-responsive SOM+ interneurons, 12/20 increased activity, $p < 0.01$ compared to excitatory pool where 47/142 increased activity, Fisher's exact test). While VIP+ interneurons showed the strongest baseline modulation, tone-evoked responses from VIP+ interneurons were muted in comparison and preferred the passive context, similar

to excitatory neurons (Fig. 3g, h). Thus, cortical interneurons are highly sensitive to behavioral context in unique ways suggesting that local inhibition may gate contextual information.

Synaptic inhibition acts as a switch to gate the flow of contextual information

Given the context-dependent neural output dynamics observed in inhibitory and excitatory networks, we wondered whether changes in excitatory-inhibitory balance might underlie the shifts in network activity. Balanced inhibition helps to control overall excitability and information processing. It may be a general property of developed cortical circuits in the auditory system^{20,24,26} and other sensory modalities^{23,35}. Co-tuning of inhibition with excitation may be disrupted in epochs of high attention or arousal and differentially affect inhibitory transmission or inhibitory neuron activity^{25,34,38–40}. Behavioral context might modulate both tone-evoked excitation and inhibition in the same direction (increasing or decreasing excitatory and inhibitory inputs together). Alternatively, changes in context might transiently disrupt excitatory-inhibitory balance, enhancing perceptual salience by selective modulation of either excitation or inhibition.

We tested these hypotheses by measuring synaptic activity onto putative excitatory neurons with whole-cell voltage-clamp recordings in behaving animals (Fig. 4a). We measured excitatory and inhibitory postsynaptic currents (EPSCs and IPSCs) in both the active and passive contexts (n=12 cells, n=4 mice). We observed significantly more context-dependent changes in IPSCs than EPSCs (Fig. 4b–e). Interestingly, the sign of inhibitory modulation was heterogeneous. In some cells, the active context enhanced tone-evoked inhibition (Fig. 4b–d), whereas inhibition was decreased in other cells, with an overall broader distribution of inhibitory changes (Fig. 4d). Comparing the absolute values of inhibitory vs. excitatory changes revealed that during the active context, IPSC amplitudes were more than twice as affected as EPSC amplitudes (Fig. 4e, IPSC: 34.9±4.1%, EPSC: 16.1±3.5%, n=12 cells, p<0.009, Student's paired two-tailed t-test, green circles denote significant changes in currents; IPSC median p-value per cell is 0.03; EPSC median p-value is 0.30; Student's paired two-tailed t-test within neuron). Tone-evoked EPSCs and IPSCs in behaving animals could be measured before the onset of licking, providing further evidence that motor-related suppression was not confounding our experiments.

We predicted firing rates using an integrate-and-fire model with our measured IPSCs and EPSCs. We observed both functional classes of neurons (activated and suppressed) that we observed with calcium imaging (Supplementary Figure 7a–c, n=5 neurons showing suppression, p<0.01, two-sided Wilcoxon rank sum test for active versus passive context; Supplementary Figure 7d–f, n=2 neurons showing activation, p<0.01, two-sided Wilcoxon rank sum test; n=5 neurons with no significant change in model-derived spiking). In two instances, we were able to record spiking activity in cell-attached configuration in the same cells where we later measured IPSCs and EPSCs after breaking in (Supplementary Figure 7g–i). In both cases, the IPSC context modulation governed whether neuronal spiking was suppressed (Supplementary Figure 7h) or activated (Supplementary Figure 7i) in the active context. Moreover, the measured spiking output (Supplementary Figure 7g–i, top row) was similar to the predicted spiking output calculated from the synaptic measurements

(Supplementary Figure 7g–i, bottom row), validating the model output. Overall, changes in inhibition can explain both response facilitation and suppression in excitatory output.

Optical inactivation of inhibitory subtypes impairs context-dependent switching

We next asked how the different elements of the inhibitory networks contribute to the context-dependent modulation between active and passive contexts, employing an optogenetic inactivation strategy (Fig. 4f–i). We expressed the hyperpolarizing opsin (eNpHR3.0) in a Cre-dependent manner in *PV-Cre*, *SOM-Cre*, and *VIP-Cre* mice in auditory cortex unilaterally.

Interestingly, optical suppression via cortical illumination of all three interneuron subtypes significantly impaired context-dependent changes in IPSCs and ultimately behavioral performance in the active context (Fig. 4g, h, Supplementary Figure 8b) implicating all three in contextual regulation. Importantly, the neuronal subtypes differed in their downstream effect on pyramidal neurons. Suppression of PV+ and SOM+ interneurons in the active context increased pyramidal neuron spiking in the active context while reducing spiking modulation between contexts (Fig. 4i, *top*; +53.4±31%, $p < 0.01$, Wilcoxon signed-rank test, $n = 9$ total (5 neurons with SOM+ inactivation, and 4 neurons with PV+ inactivation)). In contrast, suppressing VIP+ interneurons in the active context strongly decreased pyramidal neuron output (Fig. 4i, *bottom*; -93.0±6%, $p < 0.01$, Wilcoxon signed-rank test, $n = 6$ neurons). PV+ and SOM+ interneurons thus appear to directly inhibit pyramidal neurons while VIP+ interneurons disinhibit pyramidal neurons during active task engagement, suggesting that multiple interneurons are operating in parallel to achieve the observed network output.

Cholinergic tone signals a transition to the active context

Next we asked how behavioral context was initially communicated to A1 for control of network output in this complex manner. Cholinergic modulation from the nucleus basalis is a likely candidate for providing attentional signals to the auditory cortex^{25,28,38,40–45}, implicated in theoretical models^{34,39} and shown experimentally to selectively control cortical inhibition under certain conditions^{6,25,40}.

To determine how these neuromodulatory signals are regulated by behavioral context, we measured the activity of 1,600 axonal segments, including putative boutons, arising from the nucleus basalis and projecting to auditory cortex. We targeted GCaMP6s to nucleus basalis in two wild-type mice and three *ChAT-Cre* mice to specifically target cholinergic neurons (Fig. 5a–c, Supplementary Figure 9a–e). We monitored axonal activity in auditory cortex in behaving mice using two-photon calcium imaging (Supplementary Video 4). To ensure motion stability, we restricted our analysis to epochs of time (10–20 secs or 40–80 frames) in which the movement in the x-y plane was similar between the active and passive contexts. We observed clear changes in baseline activity levels of axon segments from the nucleus basalis only when switching contexts (Fig. 5b–e, $p < 10^{-4}$ within-animal comparing active to passive context baseline calcium levels, Student's paired two-tailed test). During the active context, there was a substantial increase in the tonic activity of nucleus basalis axon

segments (Fig. 5d, e, n=1,600 axonal segments in 5 mice; n=3 *ChAT-cre* animals, p<0.02, Student's paired two-tailed t-test).

If increased cholinergic modulation is critical for active task engagement, we should observe changes in cholinergic activity that predict behavioral engagement on a trial-by-trial basis. To test this, we implemented a trial-by-trial Bayesian decoder using the pre-tone baseline calcium signal in cholinergic axonal segments to predict behavioral context. We performed a two-fold cross-validation by dividing our dataset into non-overlapping training and test sets, repeating this process 1,000 times with random allocation of trials to either set. We achieved 77.9±3.9% accuracy in predicting context from these calcium signals compared to a shuffled dataset (50.6±2.0%) strongly implicating cholinergic modulation in the behavior (Fig. 5f, g). Next, we tested whether our decoder could predict key trial-to-trial variables of stimulus and action. Stimulus decoding accuracy was better-than-chance (real data versus shuffled data) only during tone presentation and not before (Supplementary Figure 9f; pre-tone, p=0.95; tone, p=0.04; post-tone, p=0.18; Student's t-test) suggesting that cholinergic terminals can carry stimulus information in a time-locked manner. Surprisingly, action decoding accuracy (lick correctly for the target tone, withholding correctly for the foil tone) was elevated even before tone onset and became significant during the tone period (Supplementary Figure 9g; pre-tone, p=0.06; tone, p=0.01; post-tone, p=0.04; Student's t-test) strongly implicating fluctuations in cholinergic terminal activity as a key driver of trial-by-trial fluctuations in performance.

Given these underlying neural dynamics of elevated cholinergic signaling in the active context, we next examined whether acetylcholine receptor activation was required for task performance. Unilateral topical application of atropine impaired performance on this task by reducing hit rate (Fig. 5h, i, atropine hit rate: 0.65±0.06 in 11 sessions, saline hit rate: 0.82±0.04 in 12 sessions, p<0.05, Student's paired two-tailed t-test, Supplementary Figure 9h, i). Trial-by-trial analysis showed that the animal's response rate was most impaired immediately after context switches (Fig. 5j). In control conditions, when transitioning to the active context, the animal's hit rate immediately reached steady state (first trial hit rate = 92±8%, steady state = 90±1.8%, p=0.85 Wilcoxon sign-rank test when comparing hit rate for trials 1–4 in the active context versus trials 11–14). In atropine conditions, the animal's hit rate started significantly lower before reaching steady state (first trial hit rate=57.1±20.2%, steady state=80.6±4.0%, p<0.05, Wilcoxon sign-rank test when comparing hit rate for trials 1–4 in the active context versus trials 11–14). We next asked whether direct activation of cholinergic terminals in auditory cortex could trigger task-like behavior even in the passive context (i.e. no licktube present, Fig. 5k–m, Supplementary Figure 10). Surprisingly, illumination of the auditory cortex in the passive context of trained animals induced tone-evoked licking. In the passive context, behavioral responses to the target tone (licking) are minimal (12±5%) but they are increased when activating cholinergic inputs to auditory cortex of trained mice (22±10%), an 80% increase in passive-context licking (Fig. 5m; n=9 sessions in 3 mice, p<0.05, Wilcoxon signed rank test). This partial restoration of active-context behavior argues that the cholinergic system plays a critical role in signaling context. Other key factors, including those that continuously update the animal on the contextual environment such as water reinforcement and somatosensation of the tongue to the licktube, likely counterbalance the cholinergic activation. Overall, these behavioral

manipulations argue that cholinergic signaling is necessary for contextual transitions and can even partially recover task-like behavior in the passive context.

Can this elevation in cholinergic tone drive the inhibitory dynamics that appear to control network output? To directly measure how this cholinergic modulation may affect layer 2/3 neurons in the auditory cortex, we performed whole-cell recordings in acute brain slices and examined the membrane potential of specific neuronal subtypes in response to a cholinergic agonist (1 μ M muscarine) while blocking NMDA, AMPA and GABA_A receptors. As suggested from previous studies in mouse barrel cortex and visual cortex^{38,40}, inhibitory interneurons were generally depolarized more during muscarine application than excitatory neurons (Fig. 6a–c; n=19 interneurons, n=15 excitatory neurons, $p < 0.001$, Student's two-tailed t-test, spikes removed). Excitatory neurons exhibited the least depolarization of all cell types (Fig. 6b, c; n=15 neurons, median depolarization: 1.6 mV, interquartile range: 0–4.3 mV); PV+ interneurons were modestly depolarized (Fig. 6b, c; PV+: n=7, +5.6mV, interquartile range: 5.1–9.4) while SOM+ and VIP+ interneurons were more strongly depolarized (Fig. 6b, c; SOM+: n=7, +8.2mV, interquartile range: 7.2–18.3; VIP+: n=5, +8.6mV, interquartile range: 3.8–9.6). These data support our calcium imaging measurements from behaving animals, given that VIP and SOM neurons exhibited the largest baseline changes in activity while PV+ neurons experienced increases in tone-evoked responses. These results, however, do not preclude network level effects of ACh on interneuron spiking; for example, ACh may act indirectly on interneuron spiking by modulating synaptic inputs, both excitatory and inhibitory, onto interneurons. Regardless, cholinergic modulation of cortical inhibition provides a powerful, cell-type selective mechanism for contextual regulation of network output and behavioral control.

Cholinergic modulation drives changes in synaptic inhibition

We then examined how cholinergic modulation directly affected excitatory and inhibitory inputs during behavior. First, we made additional whole-cell voltage-clamp recordings during behavior while applying the muscarinic acetylcholine receptor antagonist atropine (1 mM) locally to auditory cortex (Fig. 6d–f). Atropine significantly reduced contextual modulation of tone-evoked inhibition (Fig. 6e, f). Remarkably, six out of seven neurons did not show significant changes in IPSCs (Fig. 6f, IPSC: $19.7 \pm 5.6\%$, EPSC: $30.3 \pm 5.6\%$, n=7 cells, $p < 0.02$, Student's paired two-tailed t-test; green circles denote significant changes in currents, $p < 0.05$, Student's two-tailed t-test within neuron). Moreover, atropine altered the timing of synaptic inputs such that the time lag between excitation and inhibition was more variable and consistently larger than in control conditions (Supplementary Figure 11). Cholinergic activity therefore controls network activity by modulating the amplitude of inhibitory inputs and sharpening the timing of synaptic inputs.

If acetylcholine is required for contextual changes in inhibition, we reasoned that direct activation of the cholinergic system should preferentially modulate inhibition. We performed whole-cell voltage-clamp recordings in awake *Chat-ChR2* mice and optogenetically activated cholinergic terminals in A1 (Fig. 6g–i). Optogenetic release of endogenous acetylcholine desynchronized cortical activity (Supplementary Figure 12), and significantly altered tone-evoked inhibition to a greater extent than excitation (Fig. 6h, i). Similar to

context-switching, the sign of inhibitory context modulation was heterogeneous, even within the same cell. For example, at one frequency (13.5 kHz), optogenetic stimulation enhanced tone-evoked inhibition in a single neuron (Fig. 6h) while at a different frequency (26.9 kHz), optogenetic stimulation reduced tone-evoked inhibition (Fig. 6h). In either case, however, inhibition changed more than excitation (Fig. 6h, i). Overall IPSC amplitudes were nearly 50% more dynamic than EPSC amplitudes after optogenetic illumination (Fig. 6i, IPSC: $17.8 \pm 2.5\%$, EPSC: $12.6 \pm 1.7\%$, $n=5$ cells, $p < 0.03$, Student's paired two-tailed t-test; green circles denote significant changes in currents, $p < 0.05$, Student's two-tailed t-test within neuron). Taken together, our results show that cholinergic switching is required in awake mice to control cortical inhibition.

Recurrent model recapitulates network output only with parallel activation of inhibition

Our data indicate that multiple sources of inhibition are recruited in parallel by cholinergic activity to adjust input-output dynamics in the cortex. Could similar results arise from only the activation of VIP+ interneurons alone, or perhaps just the PV+ or SOM+ sub-populations? Alternatively, appropriate switching of cortical activity might arise from multiple inhibitory and disinhibitory interactions, required to generate the observed task-related modulation while maintaining an overall level of excitatory/inhibitory balance. To examine this central question requires network modeling in order to fully explore the complex dynamics between multiple cell types and neuromodulatory signaling. Thus we built a four population rate-based network model that incorporated known connectivity parameters across neuronal subtypes^{24,25} (Fig. 7a). We then simulated the effects of context switching via cholinergic modulation of all inhibitory cell types. Importantly, the model recapitulated known features of cortical responses at baseline and to sensory inputs in all cell types (Fig. 7b, bars denote model output, circles denote measured spike rates from literature^{26,28}). If the model only incorporated cholinergic activation of VIP+ interneurons, the network dynamics from the model were nearly opposite that of what we observed experimentally (Fig. 7c). Likewise, if acetylcholine only activated SOM+ or PV+ interneurons, the network dynamics were similar to the mean excitatory suppression we observed experimentally, but other circuit responses were not captured (Fig. 7c). In contrast, if acetylcholine simultaneously acted on all three interneuron subtypes, the model could recapitulate all key network responses and was robust to various changes in parameters (Fig. 7c, Supplementary Figure 13).

We analyzed the model dynamics to determine how the network state was switched by change in context. These results arise, in part, because of the inter-connectivity between interneuron subtypes. For example, cholinergic activation of PV+ neurons alone suppresses excitatory and VIP neurons, but also incorrectly suppresses SOM+ neurons. Activation of PV+ and SOM+ neurons together, overcomes the mutual suppression, but leads to direct suppression of VIP even at baseline. Activation of all three in parallel, however, creates the right balance for all three subtypes for both tone-evoked and baseline activity levels. A multi-unit rate model generated excitatory diversity about a mean suppression, including neurons with robust facilitation due to the diffuse nature of the acetylcholine signal and the underlying stochastic connectivity properties (Fig. 7d). Importantly, this diversity emerged largely due to diverse changes in inhibitory inputs (Fig. 7e). Together, the network model

provides strong theoretical foundation for parallel processing by cortical interneurons of neuromodulatory signals during behavior.

DISCUSSION

A major challenge in neural systems is to provide logic to complex neural dynamics. We present a cohesive model, based on experiments and theory, which shows how parallel processing of cholinergic modulation by diverse cortical interneurons enables the same sensory stimuli to trigger different behaviors depending on context. Surprisingly, excitatory synaptic inputs themselves are only modestly affected by context. Instead, during active engagement, cholinergic input co-activates multiple interneurons thereby adjusting inhibitory synaptic inputs and consequently modulating neuronal output. A network model captured these dynamics across neuronal subtypes only when neuromodulation coincidentally drove inhibitory and disinhibitory circuit elements, ruling out either as sole computational responses to cholinergic modulation.

Task engagement drives a continuum of responses, from suppression to facilitation, in A1

Most excitatory neurons in A1 were suppressed when the animal was engaged in the task, but many also showed response facilitation. This synthesizes findings from different groups that showed suppression during task engagement² and different forms of facilitation^{3,4}. The behavioral significance of this bidirectional modulation remains an important question. During locomotion, neuronal responses to auditory stimuli are systematically suppressed with no facilitation in the auditory cortex and the auditory thalamus^{12,17,46}. Moreover, while thalamic neurons exhibit locomotion-induced suppression, they are less sensitive to task engagement with higher cognitive load^{2,12}. Thus, facilitation of a pool of excitatory neurons appears to be cortical in nature, independent of processing earlier in the auditory pathway, and may be critical for task performance.

Imaging of inhibitory networks in the cortex demonstrated the diversity of responses both within and across interneuron sub-types. PV+ and SOM+ interneurons preferred the active context at baseline and for tone-evoked responses. In contrast, VIP+ interneurons showed large and uniform increases in baseline activity but exhibited suppressed tone-evoked responses in the active context. This suggests that inhibitory networks regulate cortical output at both a tonic and phasic level. These results are consistent with these three interneuron subtypes being sensitive to cholinergic regulation and having strong levels of interconnectivity^{6,31,47}. Most importantly, it suggests multiple interneurons are involved in regulating cortical activity during the active context.

Inhibition as a synaptic switch to control network output and context-dependent behavior

Direct recording of synaptic inputs onto single neurons during behavior is a powerful approach to dissect input-output dynamics. Our data show that inhibitory inputs were more sensitive to changes in behavioral context than excitatory inputs, under the control of cholinergic neuromodulation in a context-switching behavioral paradigm. Optical suppression of PV+ and SOM+ neurons during active behavior increased layer 2/3 pyramidal neuron output, implicating these neurons in suppression of excitatory output. In

contrast, optical suppression of VIP+ interneurons during active behavior decreased layer 2/3 pyramidal output, implicating these neurons in disinhibition. Moreover, unilateral optogenetic suppression of any of these interneurons reduced the strength of contextual modulation of IPSCs and impaired task performance. This shows that multiple interneurons play a key role in gating contextual information.

Cholinergic signaling activates multiple interneurons in parallel during behavior

Task engagement was conveyed to the cortex by the cholinergic projections of the nucleus basalis. Calcium imaging of neuromodulatory axons in recipient regions, such as the auditory cortex, allows us to better understand how neuromodulatory systems selectively engage during behaviorally relevant epochs. In the context-switching behavioral paradigm, the activity of cholinergic axons from the nucleus basalis increased during task engagement. We showed in cortical brain slices that a cholinergic agonist (muscarine) depolarized inhibitory interneurons significantly more than excitatory neurons. Our data does not preclude the possibility that other basal forebrain projections that release GABA, glutamate, or peptides may also show differences in activity⁴⁸. However, we note that blocking cortical muscarinic acetylcholine receptors reduced changes in IPSCs and impaired behavioral performance, suggesting that cholinergic modulation of synaptic inhibition is critical for control of cortical state. Moreover, tone-evoked licking could be partially recovered in the passive context by optically activating cholinergic axons in the auditory cortex of trained mice. Our focus has been on the activation of muscarinic receptors in cortical neurons. A complementary and important future avenue of work will further dissect the role of nicotinic receptor activation. This further dissection may also show that cholinergic activity may impact other important mechanisms for task-related responses, including modulation of thalamocortical activity⁴⁹.

These findings complement recent work showing how phasic responses of cholinergic neurons³⁰. The cholinergic system likely modulates behavior both by setting the contextual tone and providing rapid phasic signals during behavior³⁰. Our findings, however, do not preclude a role for other neuromodulatory centers or long-range cortical connections from influencing context-dependent activity in auditory cortex. In addition, basal forebrain projections to the visual cortex have been shown to yield opposite direction of modulation; namely, visual cortical neurons show increased activity during cholinergic stimulation⁵⁰. These cortical differences may arise due to the preferential and region-specific innervation of specific subtypes of interneurons^{7,31}. Moreover, it is likely that other key neuromodulatory centers may be critical for maintaining full performance. Other circuits may impinge on cortical circuits to further influence this switching time as well as steady-state performance. Overall, these results show how cortical inputs and outputs are transformed by behavioral context. Parallel processing by diverse cortical interneurons of long-range inputs may therefore be a general feature of cortical activity during cognitive behaviors.

ONLINE METHODS

Surgical preparation

All procedures were approved under an NYU IACUC protocol. To generate PV-tdTomato, SOM-tdTomato and VIP-tdTomato mice, PV-cre, SOM-cre, and VIP-cre animals were crossed with the Ai9 (Allen Institute) tdTomato-flox reporter line. ChAT-cre mice were used for imaging cholinergic axon terminals (JAX) and ChAT-ChR2 mice were used for optogenetic experiments. C57/BL6 mice were used in all other experiments. In all cases, male and female mice 2–3 months old were anesthetized with isoflurane (2.0% during induction and surgery, 0.75% during physiology). A craniotomy was performed over the temporal lobe to expose the auditory cortex (3 mm craniotomy, centered 1.75 mm anterior to the lambda suture on the ridge line). Pure tones at 70 dB SPL and 4–64 kHz frequencies (50 msec, 3 msec cosine on/off ramps, quarter-octave spacing) were delivered in pseudo-random sequence at 0.5–1 Hz. The location of A1 was determined by mapping multiunit responses 500–700 μm below the surface using tungsten electrodes in a sound-attenuating chamber. An adeno-associated virus (AAV) vector encoding the calcium indicator GCaMP6s (AAV1-SYN-GCaMP6s, UPENN vector core) was injected for expression in layer 2/3 neurons in right A1 (n=5 mice for Fig. 2a–e; in Fig. 3, n=2 mice for PV-tdTomato, n=2 mice for SOM-tdTomato, and n=2 mice for VIP-tdTomato). For isolation of excitatory neurons, we used an AAV encoding the calcium indicator GCaMP6f (AAV9.CamKII.GCaMP6f) (n=2 mice). Above the injection coordinates, a cranial window was implanted replacing a circular piece of skull by a glass coverslip (diameter of 3 mm, Warner Instruments) that was secured in place using a mix of dental cement and Crazy Glue. A custom-made stainless-steel headpost (Ponoko) was affixed to the skull using C&B Metabond dental cement (Parkell). A small burr hole was drilled anterior to bregma and a ground wire was placed under the skull above the pial surface. The ground wire was then connected to the metal headpost to allow for lick-detection. Each animal was allowed to recover for at least 2–3 weeks.

For experiments imaging the activity of axonal projections from the basal forebrain, we carefully leveled the head and drilled a small burr hole targeting the right nucleus basalis (AP, –0.5 mm; ML, 1.8 mm; DV, 4.5 mm). We injected 1.5 μl of an AAV vector encoding the calcium indicator AAV1-SYN-GCaMP6s (U. Penn vector core) into C57 mice (JAX), or 1.5 μl of AAV1-SYN-FLEX-GCaMP6s (U. Penn vector core) into *ChAT-Cre* mice to specifically target cholinergic neurons. We injected at a rate of 100 nl/min and waited 15 minutes before extracting the injection needle. We filled the burr hole with bone wax and sealed it with dental cement.

Behavioral training and control for imaging experiments

All behavioral events (imaging time-stamping, stimulus delivery, water delivery, and lick detection) were monitored and controlled by custom-written programs in MATLAB interfacing with an RZ6 auditory processor (Tucker-Davis Technologies). Training began after at least 7 days of water restriction. Training took place during the day and began with habituation to head-fixation, which was immediately followed by water-sampling sessions while animals were immobilized in a plexiglass tube. Mice typically learned to lick aggressively for 3–5 μl droplets of water within 1–2 sessions. Once the animals would lick

reliably, they were immediately placed in the complete behavioral task with minimal shaping. We utilized a go/no-go behavior task with the target and foil chosen based on the two-photon targeted imaging. Importantly, the initial training session included passive context behavior (i.e., the tones but no behavioral responses), as animals would continue to lick even in the absence of the lick tube if the passive context was not introduced early in the training procedure. For active context, a behavioral block typically consisted of 100 trials with 4 blocks of training conducted per day (total of ~400 trials per day). Target versus foil trials were pseudo-randomly ordered, each of which consisted of scan onset (imaging), pre-stimulus period (1.25 s), stimulus period (500 ms), delay (250 ms), a response period (1.75 s), and an inter-trial interval (ITI with variable duration as described below). Mice only received water for correct responses to the target during the response period. Incorrect licks recorded after the foil presentation (a false alarm) were mildly punished by increasing the ITI. Animals were not punished if they licked during any other time epoch (i.e., if animal licked in the pre-stimulus period, tone presentation or delay period, the trial continued). This enabled us to confirm that animals were actively increasing lick rate for target tones during hit trials and reducing lick rate for foil tones during correct rejects (from baseline lick rate to zero during response window). This measurement confirmed that both the target and foil tone had behavioral effects on the animal; without this, animals could take a single-tone strategy (i.e., learn to lick only for the target tone or withhold licking for the foil tone).

Hit trial ITIs were 4–5 s (to enable full licking of reward), miss trials were not punished and had an ITI of 2–3 s, false alarm trials were punished with an ITI lasting 7–9 s, and correct rejects immediately moved to the next trial with an ITI of 2–3 s. Passive context was initiated immediately after completion of active context trial blocks. For layer 2/3 imaging experiments in Fig. 2, a chamber light cue was briefly turned on, the lick tube was rotated out of place, and the light turned back off. Care was taken to not physically alter the position of the animal. For cell-type specific imaging including excitatory neurons, interneuron imaging (Fig. 3) and axonal imaging of *ChAT-cre* animals (Fig. 5), lick tube removal was automated using a micromanipulator and images were acquired for the entire duration of the experiment. For physiology experiments (Figs. 4–6, Supplementary Figure 11), lick tube removal was performed within 5–10s either manually or with an automated actuator and licks were detected with an infrared beam. In a subset of mice, licking was monitored using an infrared camera or beam to determine whether presentation of sound stimuli elicited a licking movement from the animal. Only in rare cases did mice lick for the target tone in the absence of the lick tube and if it did, this behavior only lasted for 1–2 trials. In a subset of animals (n=2), we established that the animals were still thirsty immediately after the passive trial, i.e., the animals would lick for ad-libitum access to water, confirming that any changes in neuronal responses were not due to “satiety”..

For muscimol experiments, animals were injected bilaterally with either saline vehicle or muscimol (1 μ L of 1 mg/mL) at a depth of ~600 μ m below the pial surface. The drug was allowed to diffuse while the animals were head-fixed for 10–15 minutes before behavior was initiated. In all cases, animals were tested with either saline injection or no injection the day after muscimol injections to determine if behavior recovered.

Behavior for physiology experiments

For physiology experiments, animals were trained on target and foil that were pre-selected before any physiological recordings (target=9.5 kHz, foil=5.6 kHz, 0.75 octave spacing). Given the typically shorter durations of whole-cell recordings, passive presentation was restricted to the target and foil, and lick tube removal (from active-to-passive) or insertion (passive-to-active) was performed in 5–7 s using either a manual manipulator or automated linear actuator. On the day immediately preceding whole-cell recordings, animals performed with $d' > 1.5$. Tone duration was set to 100 ms for training and experimentation. During training, hit ITIs were 4–5 s (to enable full licking of reward), miss trials were not punished and had an ITI of 2–3 s, false alarm trials were punished with an ITI lasting 7–9 s, and correct rejects immediately moved to the next trial with an ITI of 2–3 s. After animals were trained, false alarms were no longer punished during whole-cell recordings in order to maximize the number of trials while recordings were stable.

In vivo calcium imaging

Two-photon fluorescence of GCaMP6s was excited at 900 nm using a mode locked Ti:Sapphire laser (MaiTai, Spectra-Physics, Mountain View, CA) and detected in the green channel (GFP emission). Imaging was performed on a multiphoton imaging system (Moveable Objective Microscope, Sutter Instruments) equipped with a water immersion objective (20X, NA=0.95, Olympus) and the emission path was shielded from external light contamination. Images were collected using ScanImage (HHMI). To image auditory cortex, the objective was tilted to an angle of 50–60°. To record time courses of auditory-evoked neuronal activity, awake animals were head-fixed under the microscope and a speaker was placed adjacent to the microscope (microphone-ear distance ~10 cm). During auditory stimulation, ~300 μm^2 areas in layer 2/3 of A1 containing multiple GCaMP6s expressing neurons were selected and imaged (scan rate ~4 Hz, 0.26 s/frames, laser power 40 mW). For passive context, pure tones (70 dB SPL, 4–64 kHz, 500 msec, 10 msec cosine on/off ramps, quarter-octave spacing) were delivered in pseudo-random sequence every 20 frames (~5s per passive context trial).

Motion correction

We used a multi-step approach to compensate for x-y motion due to movements of the awake mouse. First, we performed a frame-by-frame, rigid registration of the imaging frames that accounts for x-y changes in displacement, rotation and translation. Similar to published reports, a mean luminance-stable epoch from the middle of the session was chosen as the reference frame⁵³. Second, in animals with a structural marker (tdTomato in PV+ and VIP+ interneurons) we separated the functional channel (green, GCaMP6s) from the structural channel (red, tdTomato). We then computed the tone-evoked response for both the fluorescent signal from the functional green channel (GCaMP6s) and the structural red channel (tdTomato). The red channel (tdTomato) had a small amount of fluorescence bleedthrough from the green fluorophore (GCaMP6s) that we could spectrally resolve using linear unmixing. We excluded data when the red channel exhibited stimulus-evoked “transients” that could not be explained by fluorescence bleedthrough (Supplementary Figure 6). Third, in animals without a structural marker, we assessed the probability of

with 95%/5% O₂/CO₂ (pH 7.4). Slices (300–400 μm thick) were prepared with a vibratome (Leica), placed in warm dissection buffer (33–35° C) for <30 min, then transferred to a holding chamber containing warmed artificial cerebrospinal fluid (ACSF) (in mM: 124 NaCl, 2.5 KCl, 1.5 MgSO₄, 1.25 NaH₂PO₄, 2.5 CaCl₂, and 26 NaHCO₃). Slices were kept at room temperature (22–24° C) for >25 minutes before use. For experiments, slices were transferred to the recording chamber and perfused (2–2.5 ml min⁻¹) with oxygenated ACSF at 33° C.

Somatic whole-cell recordings were made from layer 2/3 pyramidal cells. Recordings were performed in current-clamp mode with a Multiclamp 700B amplifier (Molecular Devices) using IR-DIC video microscopy (Olympus). Patch pipettes (5–8 MΩ) were filled with intracellular solution (in mM: 135 K-gluconate, 5 NaCl, 10 HEPES, 5 MgATP, 10 phosphocreatine, and 0.3 GTP). For blocking synaptic activity, we used DNQX (10 mM), APV (25 mM), Picrotoxin (10 mM), and 1–2 μM muscarine. The mean series resistance (R_s) was 27.4±10.4 MΩ (standard deviation, s.d.) and the mean input resistance (R_i) was 88.7±25.8 MΩ, determined by monitoring cells with hyperpolarizing pulses (40 pA for 50 msec). Recordings were excluded from analysis if R_s or R_i changed >30% compared to the baseline period. Data were digitized at 10 kHz and analyzed with Clampfit 10 (Molecular Devices). Picrotoxin, DNQX, and APV were purchased from Sigma. All statistics and error bars are reported as means±s.e.m. and statistical significance assessed with paired two-tailed Student's t-tests.

In Vivo Electrophysiology

In vivo whole-cell recordings were performed in a sound-attenuating chamber, and recordings obtained from auditory cortical neurons with a Multiclamp 700B amplifier (Molecular Devices). For voltage-clamp recordings, pipettes contained: 130 Cs-methanesulfonate, 1 QX-314, 4 TEA-Cl, 0.5 BAPTA, 4 MgATP, 20 phosphocreatine, 10 HEPES, pH 7.2. Whole-cell recordings from A1 neurons were obtained from cells located within 400 μm of the pial surface, in putative layer 2/3. Data were filtered at 5 kHz, digitized at 20 kHz, and analyzed with Clampfit 10 (Molecular Devices). R_s : 47.4±31.6 MΩ; R_i : 154±150 MΩ (s.d.) in 38 cells. Recordings were excluded from analysis if R_s or R_i changed >30% relative to the either passive or active context. For all included cells, we also examined the correlation between changes to synaptic currents and changes to R_i and R_s , for both IPSCs and EPSCs and observed no correlation (IPSC: $r=-0.13$, $p=0.62$ for R_s , $r=-0.17$, $p=0.51$ for R_i ; EPSC: $r=-0.06$, $p=0.82$ for R_s , $r=-0.05$, $p=0.85$ for R_i). We utilized a preparation which enabled access to auditory cortex via a ~200 μm hole in a 3 mm piece of round glass, providing the stability required to hold cells across conditions⁵⁴ (Fig. 4a).

Pure tones (100 msec duration, 3 msec cosine on/off ramps) for target and foil (5–10 kHz) were played at 70 dB SPL. Tone-evoked responses were measured in a tone onset and offset window (150 ms) starting at tone onset. Power analysis was performed to determine sample size for statistical significance with a power of β:0.7; these studies required at least three neurons for differences in synaptic currents during regular behavior between contexts, five neurons for pharmacology experiments, and three neurons for optogenetics experiments, all satisfied in the experiments of Figs. 4,6 and Supplementary Figure 11. For all patch-clamp

experiments, IPSCs and EPSCs values were calculated using the peak amplitude during the tone (for tone onset neurons) or during and immediately after the tone (for tone offset neurons). The modulation index was calculated relative to the active context (Active-Passive)/Active.

For atropine experiments, 1 mM atropine was topically applied through a hole in the cranial window for at least 30 minutes prior to patch-clamp experiments or behavior; control experiments were performed with saline. For cholinergic modulation via optogenetic stimulation in *ChAT-ChR2-EYFP* mice, blue light was delivered to the brain surface via a 200 μm fiber (Thorlabs) positioned ~ 0.5 mm above the brain surface, coupled to a 473 nm laser (CrystaLaser). During whole-cell recordings, blue light pulses were triggered 100 ms before tone onset and lasted for 375 ms (473 nm wavelength, 2–2.5 mW) at the surface of the brain. During desynchronization experiments (Supplementary Figure 12), 473 nm light was delivered in a 5 sec square pulse at 5 mWmm^{-2} . LFP recordings were made using a 0.5 M Ω tungsten electrode, and were acquired at 20 kHz. For spectral analysis in Supplementary Figure 12, we down-sampled LFP recordings to 200 Hz, then performed time-frequency decomposition of the LFP using custom software written in Matlab. We used a 1 s sliding window with 50 ms steps and averaged spectra across trials. The spectra shown in Supplementary Figure 12 were obtained from 10 trials of 5 sec square laser pulses delivered to auditory cortex. Each frequency band was normalized by the average power in the 2 s baseline period preceding cortical optical stimulation. Changes in synaptic responses in Figs. 4,5 and Supplementary Figures 8, 11 were compared by Student's paired two-tailed t-tests as data passed Kolmogorov-Smirnov normality tests.

For interneuron inactivation experiments, AAV1.EF1a.DIO.eNpHR3.0 was injected unilaterally into the auditory cortex of *PV-cre*, *SOM-cre*, or *VIP-cre* mice at least 2 weeks prior to any electrophysiological or optogenetic experiments. On the first day of recording, we removed the skull only above auditory cortex and implanted a cranial window for optical illumination with a small access hole for the patch electrode. We then restricted optical illumination to auditory cortex with a fiber-coupled laser. During whole-cell recordings or behavioral sessions, blue light pulses were triggered 100 ms before tone onset and lasted for 300 ms (532 nm wavelength, 10–20 mW/mm^2) at the surface of the brain.

Integrate-and-fire model of synaptic currents

The simulations in Supplementary Figure 7 used a conductance-based integrate-and-fire model neuron similar to our previous study relating synaptic currents and spike generation²⁸. For simulating the spiking patterns of each cell, we used EPSCs and IPSCs from experiments in Fig. 4. On each trial, one EPSC and one IPSC were randomly chosen from the set of recorded responses. Excitatory and inhibitory synaptic conductances (g_e and g_i respectively) were computed from currents as previously described²⁸, and then g_e and g_i were randomly rescaled on each trial to have peak instantaneous conductance over the range 1.0–1.7 nS. Membrane voltage was computed as:

$\tau_m \frac{dV}{dt} = V_{rest} - V + g_e(t)(E_e - V) + g_i(t)(E_i - V)$, with $\tau_m = 10$ ms, resting membrane potential $V_{rest} = -70$ mV, excitatory reversal potential $E_e = 0$ mV, and inhibitory reversal potential $E_i = -70$ mV. A spike was evoked in the postsynaptic neuron if the membrane

voltage reached threshold of -40 mV, at which point the membrane potential was reset to -80 mV in the next time step. Spike rates and trial-by-trial correlation were determined over 100–200 trials (to ensure sampling from the full set of EPSCs and IPSCs), and full rasters for all modeled trials are displayed in Supplementary Figure 7c for each simulation. Code can be obtained at: http://froemkelab.med.nyu.edu/kuchibhotla_etal_simulations.

Network model: 4-unit Model

We built a circuit model of auditory cortex containing four populations: one excitatory and one for each of the three inhibitory subtypes (PV, VIP, and SOM). Each population is represented by a single rate-based equation:

$$\tau_x \frac{dr_x}{dt} = -r_x + f(I_x^{tot})$$

with

$$I_x^{tot} = \sum_y W_{xy} r_y + I_x^B + I_x^T + I_x^A$$

where r_x is the firing rate of the X cell population (with X=E,P,V,S). The time constants were the same for all I subtypes ($\tau_{P,V,S} = 10$ ms) and slower for the E population ($\tau_E = 20$ ms). f is the neural activation function. Here we use a rectified power-law (Miller and Troyer, 2002):

$$f(I_x^{tot}) = k([I_x^{tot}]_+)^n$$

with $k = .01$ and $n = 2.2$. Use of a rectified linear activation function ($k = 1$, $n = 1$) provided qualitatively similar results.

Connections between populations are given via a weight matrix:

$$W = \begin{bmatrix} W_{EE} & W_{EP} & W_{EV} & W_{ES} \\ W_{PE} & W_{PP} & W_{PV} & W_{PS} \\ W_{VE} & W_{VP} & W_{VV} & W_{VS} \\ W_{SE} & W_{SP} & W_{SV} & W_{SS} \end{bmatrix}$$

Values for inhibitory connections were determined using data from visual cortex (Pfeffer et al., 2013), with the addition of a VIP to PV connection known to exist in auditory cortex (Pi et al., 2013) (note, the results do not depend on this connection). Values for excitatory connections were determined from empirical and modeling studies (Hofer et al., 2011, Litwin-Kumar et al., 2016), and all weights were fit to ensure they produced reasonable firing rates. This produced the following set of values:

$$W = \begin{bmatrix} .017 & -.956 & -.045 & -.512 \\ .8535 & -.99 & -.09 & -.307 \\ 2.104 & -.184 & 0 & -.734 \\ 1.285 & 0 & -.14 & 0 \end{bmatrix}$$

Constant background input is given to all four populations in order to create reasonable spontaneous rates (IEB=12.8, IPB=24, IVB=8, ISB=9.6). Tone-related input is given only to the excitatory and PV populations, for the duration of the tone (IET=93, IPT=74, 100ms) (Ji et al., 2016). The strength of the tone-related inputs were chosen such that they elicited tone-evoked firing rates in each of the four populations that were consistent with reported rates in auditory cortex (Chen et al., 2015, Mesik et al., 2015).

For modeling of the passive condition, no Ach inputs are given (IA=0). In the active condition, the effects of Ach are modeled as a small additional input to all three inhibitory populations (unless otherwise noted), based on the reported depolarizing effects of Ach on these cell types (IpA = IVA = ISA = 5, though the results are robust to differences in IA across subtypes (Supplementary Figure 13). Spontaneous and evoked rates in both conditions were determined using steady state values of the model. However, measuring tone-evoked rates using either peak values or rates averaged over the initial tone-evoked transients (50ms) produced qualitatively similar results.

To test for robustness, the following parameters of the model were varied independently from -10% to +10% of their current values: IET, IPT, IpA, IVA, ISA, and all nonzero entries of W. Out of 5000 simulations run with these randomly chosen parameters, all but one produced correct directional changes due to Ach in all four cell types. Thus, the model is robust to parameter variations in this range. All simulations were run using the forward Euler method with 0.5ms time step.

Network model: multi-unit

In order to explore diversity within a cell type population, the four unit model described above was expanded into a multi-unit model, wherein each cell subtype was represented by multiple individual rate-based units rather than just one. The number of cells per population varied by subtype (NE=800, NP=100, NV=50, NS=50). Assuming the following connection probabilities between subtypes (though results are comparable for a range of connection probabilities):

$$P = \begin{bmatrix} .15 & .3 & .3 & .3 \\ .3 & .3 & .3 & .3 \\ .3 & .3 & 0 & .3 \\ .3 & 0 & .3 & 0 \end{bmatrix}$$

The mean synaptic strength between different cell types was calculated by dividing the weight between the cell types by the product of the connection probability and the number of cells in the presynaptic population: $G_{XY} = W_{XY} / (N_Y * P_{XY})$. This gives:

$$G = \begin{bmatrix} .0001 & -.0319 & -.0030 & -.0341 \\ .0036 & -.0330 & -.0060 & -.0205 \\ .0083 & -.0061 & 0 & -.0489 \\ .0054 & 0 & -.0093 & 0 \end{bmatrix}$$

Actual synaptic strengths were drawn from a lognormal distribution with the given mean and variance equaling one-ninth the mean. (Note, the mean E to VIP connection was lowered slightly as compared to the 4-unit model, as it provided a better fit to the desired firing rates in the multi-unit model).

Similar to the 4-unit model, background input was given to all cells to maintain reasonable spontaneous rates with values as in the 4-unit model. Tone inputs were given to all E and PV cells only; tone-related inputs were drawn independently for each cell on each trial from a Gaussian with mean values as in the 4-unit model and a variance of 2. Ach inputs were given to all PV, VIP, and SOM cells but drawn independently for each cell, and held constant across trials, from a Gaussian with a mean value of 5 and variance of 10 (truncated so that all values remain positive). This variance of cholinergic effects was intended to represent the likely variability in the nature of cholinergic innervation in auditory cortex.

Results were calculated using 20 realizations of the network, run with 15 trials each for passive and active conditions. The multi-unit model matches the 4-unit model in terms of average spontaneous and evoked firing rates, and average changes in firing rate due to Ach.

Histology

To confirm the specific expression of the genetically encoded calcium indicator GCaMP6s in nucleus basalis cholinergic neurons following injection in ChAT-Cre mice, we performed ChAT immunohistochemistry. We performed similar histology with different antibodies to confirm eNpHR3.0 expression in interneuron Cre lines and selective expression of CAMK2-GCaMP6f in excitatory neurons preferentially (Supplementary Figure 14). Mice were transcardially perfused using ~45 mL PBS followed by ~45 mL 4% PFA under deep anesthesia. Brains were extracted from the skull and post-fixed in 4% PFA for ~2 hours at 4°C, then cryoprotected overnight in 30% sucrose solution and sliced coronally with 16 µm thickness on a cryostat. Fixed brain sections were washed with PBS, then incubated for 2–3 hours at room temperature in blocking buffer containing PBS with 0.5% v/v Triton X-100 (Sigma), 2% v/v normal goat serum (Life Technologies) and 50 mg/mL BSA. The blocking solution was aspirated and the slices were incubated in primary antibody (1:1000 dilution of chicken anti-GFP IgY, catalog # ab13970 (Abcam); 1:200 rabbit anti-ChAT IgG, cat. # AB143 (Millipore); 1:1000 dilution of VIP antibody IgG, product. #20077 (Immunostar); 1:1000 dilution of anti-parvalbumin IgG, code #235 (Swant); 1:500 dilution of anti-somatostatin IgG, clone YC7, cat. #MAB354 (Millipore)) overnight at 4°C. Afterwards, slices were washed and incubated for 1–2 hours at room temperature in secondary antibody (1:1000 dilution, goat anti-chicken IgY Alexa Fluor 488, cat. # A11039; goat anti-rabbit IgG Alexa Fluor 555, cat. # A21430, both from Life Technologies; 1:1000 dilution of goat anti-mouse IgG Alexa Fluor 555, cat. #A21422 (Life Technologies); 1:500 dilution of goat anti-

rat IgG, Alexa Fluor 555, cat. #A21434 (Life Technologies)). Finally, slides were washed, incubated at room temperature in DAPI/Hoechst solution (1:1000 in PBS), washed, then coverslipped using Fluoromount (Sigma). Images were acquired from nucleus basalis with a 20x air objective on a Zeiss LSM 710 Confocal Microscope (Carl Zeiss Inc.) and cell counts were performed in Image J (NIH). All cells stained with both anti-ChAT and anti-GFP antibodies were considered cholinergic and expressing GCaMP6s. Overall, $95.2 \pm 2.6\%$ ($n=3$ mice) of GCaMP6s+ cells were ChAT+ ($n=3$ mice, 15 images), and 50% of ChAT+ cells were GCaMP6s+ ($n=3$ mice, 15 images). All cells counted had confirmed nuclear DAPI staining.

Statistical analysis

All statistical analyses were performed in MATLAB or GraphPad Prism 6. Datasets were tested for normality, and appropriate statistical tests applied as described in the text (e.g., t-test for normally distributed data, Fischer's exact test for categorical observations, Mann Whitney U-test for non-parametric data, Friedman test with Dunn post-hoc for non-parametric data with repeated measurements). Shaded regions surrounding line-plots indicate \pm s.e.m unless otherwise stated. Unless otherwise indicated in the methods, no statistical methods were used to pre-determine sample sizes but our sample sizes are similar to those reported in previous publications^{7,8,48,53}. Data collection and analysis were not performed blind to the conditions of the experiments.

Code and Data availability

All code related to the modeling work is available at <http://froemkelab.med.nyu.edu/>. The data that support the findings of this study are available from the corresponding author upon request.

Supplementary Material

Refer to Web version on PubMed Central for supplementary material.

Acknowledgments

We thank I. Carcea, G. Fishell, B. Kripkee, M. Long, M. Picardo, D. Rinberg, R. Tsien and D. Vallentin for comments on earlier versions of this manuscript; K. Katlowitz, X. Lin, H. Lu, J. Merel, and L. Paniniski for assistance with statistics and analysis; and G. Kosche, E. Morina, A. Resulaj, and C. Wilson for technical assistance. We thank the GENIE Program and the Janelia Farm Research Campus, Howard Hughes Medical Institute for provision of GCaMP6s and ScanImage. Artwork in Figures 1, 4, and 6 was made by S.E. Ross. This work was funded by grants from NIDCD (DC009635 and DC012557), a Sloan Research Fellowship, and a Klingenstein Fellowship (R.C.F.); and NIDA (T32 DA007254), the Charles H. Revson Senior Fellowship in Biomedical Sciences, and the NIDCD (DC05014) (K.V.K.).

REFERENCES AND NOTES

1. Fritz J, Shamma S, Elhilali M, Klein D. Rapid task-related plasticity of spectrotemporal receptive fields in primary auditory cortex. *Nature neuroscience*. 2003; 6:1216–1223. DOI: 10.1038/nn1141 [PubMed: 14583754]
2. Otazu GH, Tai LH, Yang Y, Zador AM. Engaging in an auditory task suppresses responses in auditory cortex. *Nature neuroscience*. 2009; 12:646–654. DOI: 10.1038/nn.2306 [PubMed: 19363491]

3. Atiani S, et al. Emergent selectivity for task-relevant stimuli in higher-order auditory cortex. *Neuron*. 2014; 82:486–499. DOI: 10.1016/j.neuron.2014.02.029 [PubMed: 24742467]
4. Rodgers CC, DeWeese MR. Neural correlates of task switching in prefrontal cortex and primary auditory cortex in a novel stimulus selection task for rodents. *Neuron*. 2014; 82:1157–1170. DOI: 10.1016/j.neuron.2014.04.031 [PubMed: 24908492]
5. Leonard MK, Chang EF. Dynamic speech representations in the human temporal lobe. *Trends in cognitive sciences*. 2014; 18:472–479. DOI: 10.1016/j.tics.2014.05.001 [PubMed: 24906217]
6. Letzkus JJ, et al. A disinhibitory microcircuit for associative fear learning in the auditory cortex. *Nature*. 2011; 480:331–335. DOI: 10.1038/nature10674 [PubMed: 22158104]
7. Fu Y, et al. A cortical circuit for gain control by behavioral state. *Cell*. 2014; 156:1139–1152. DOI: 10.1016/j.cell.2014.01.050 [PubMed: 24630718]
8. Niell CM, Stryker MP. Modulation of visual responses by behavioral state in mouse visual cortex. *Neuron*. 2010; 65:472–479. DOI: 10.1016/j.neuron.2010.01.033 [PubMed: 20188652]
9. David SV, Fritz JB, Shamma SA. Task reward structure shapes rapid receptive field plasticity in auditory cortex. *Proceedings of the National Academy of Sciences of the United States of America*. 2012; 109:2144–2149. DOI: 10.1073/pnas.1117717109 [PubMed: 22308415]
10. Tabossi P. Effects of Context on the Immediate Interpretation of Unambiguous Nouns. *J Exp Psychol Learn*. 1988; 14:153–162. DOI: 10.1037/0278-7393.14.1.153
11. Gennari SP, MacDonald MC, Postle BR, Seidenberg MS. Context-dependent interpretation of words: Evidence for interactive neural processes. *Neuroimage*. 2007; 35:1278–1286. DOI: 10.1016/j.neuroimage.2007.01.015 [PubMed: 17321757]
12. Williamson RS, Hancock KE, Shinn-Cunningham BG, Polley DB. Locomotion and Task Demands Differentially Modulate Thalamic Audiovisual Processing during Active Search. *Current biology: CB*. 2015; 25:1885–1891. DOI: 10.1016/j.cub.2015.05.045 [PubMed: 26119749]
13. Jaramillo S, Borges K, Zador AM. Auditory Thalamus and Auditory Cortex Are Equally Modulated by Context during Flexible Categorization of Sounds. *The Journal of neuroscience: the official journal of the Society for Neuroscience*. 2014; 34:5291–5301. DOI: 10.1523/JNEUROSCI.4888-13.2014 [PubMed: 24719107]
14. McGinley MJ, David SV, McCormick DA. Cortical Membrane Potential Signature of Optimal States for Sensory Signal Detection. *Neuron*. 2015; 87:179–192. DOI: 10.1016/j.neuron.2015.05.038 [PubMed: 26074005]
15. Miller JM, et al. Single cell activity in the auditory cortex of Rhesus monkeys: behavioral dependency. *Science*. 1972; 177:449–451. [PubMed: 4625421]
16. Hubel DH, Henson CO, Rupert A, Galambos R. Attention units in the auditory cortex. *Science*. 1959; 129:1279–1280. [PubMed: 13658956]
17. Zhou M, et al. Scaling down of balanced excitation and inhibition by active behavioral states in auditory cortex. *Nature neuroscience*. 2014; 17:841–850. DOI: 10.1038/nn.3701 [PubMed: 24747575]
18. Kato HK, Gillet SN, Isaacson JS. Flexible Sensory Representations in Auditory Cortex Driven by Behavioral Relevance. *Neuron*. 2015; 88:1027–1039. DOI: 10.1016/j.neuron.2015.10.024 [PubMed: 26586181]
19. Tan AY, Wehr M. Balanced tone-evoked synaptic excitation and inhibition in mouse auditory cortex. *Neuroscience*. 2009; 163:1302–1315. DOI: 10.1016/j.neuroscience.2009.07.032 [PubMed: 19628023]
20. Wehr M, Zador AM. Balanced inhibition underlies tuning and sharpens spike timing in auditory cortex. *Nature*. 2003; 426:442–446. DOI: 10.1038/nature02116 [PubMed: 14647382]
21. Volkov IO, Galazjuk AV. Formation of spike response to sound tones in cat auditory cortex neurons: interaction of excitatory and inhibitory effects. *Neuroscience*. 1991; 43:307–321. [PubMed: 1922775]
22. Anderson JS, Carandini M, Ferster D. Orientation tuning of input conductance, excitation, and inhibition in cat primary visual cortex. *Journal of neurophysiology*. 2000; 84:909–926. [PubMed: 10938316]

23. Ferster D. Orientation selectivity of synaptic potentials in neurons of cat primary visual cortex. *The Journal of neuroscience: the official journal of the Society for Neuroscience*. 1986; 6:1284–1301. [PubMed: 3711980]
24. Froemke RC. Plasticity of cortical excitatory-inhibitory balance. *Annual review of neuroscience*. 2015; 38:195–219. DOI: 10.1146/annurev-neuro-071714-034002
25. Froemke RC, Merzenich MM, Schreiner CE. A synaptic memory trace for cortical receptive field plasticity. *Nature*. 2007; 450:425–429. DOI: 10.1038/nature06289 [PubMed: 18004384]
26. Marlin BJ, Mitre M, D'Amour JA, Chao MV, Froemke RC. Oxytocin enables maternal behaviour by balancing cortical inhibition. *Nature*. 2015; 520:499–504. DOI: 10.1038/nature14402 [PubMed: 25874674]
27. Kuhlman SJ, et al. A disinhibitory microcircuit initiates critical-period plasticity in the visual cortex. *Nature*. 2013; 501:543–546. DOI: 10.1038/nature12485 [PubMed: 23975100]
28. Bakin JS, Weinberger NM. Induction of a physiological memory in the cerebral cortex by stimulation of the nucleus basalis. *Proceedings of the National Academy of Sciences of the United States of America*. 1996; 93:11219–11224. [PubMed: 8855336]
29. Kilgard MP, Merzenich MM. Cortical map reorganization enabled by nucleus basalis activity. *Science*. 1998; 279:1714–1718. [PubMed: 9497289]
30. Hangya B, Ranade SP, Lorenc M, Kepecs A. Central Cholinergic Neurons Are Rapidly Recruited by Reinforcement Feedback. *Cell*. 2015; 162:1155–1168. DOI: 10.1016/j.cell.2015.07.057 [PubMed: 26317475]
31. Pi HJ, et al. Cortical interneurons that specialize in disinhibitory control. *Nature*. 2013; 503:521–524. DOI: 10.1038/nature12676 [PubMed: 24097352]
32. Chubykin AA, Roach EB, Bear MF, Shuler MG. A cholinergic mechanism for reward timing within primary visual cortex. *Neuron*. 2013; 77:723–735. DOI: 10.1016/j.neuron.2012.12.039 [PubMed: 23439124]
33. Lovett-Barron M, et al. Dendritic inhibition in the hippocampus supports fear learning. *Science*. 2014; 343:857–863. DOI: 10.1126/science.1247485 [PubMed: 24558155]
34. Vogels TP, Abbott LF. Gating multiple signals through detailed balance of excitation and inhibition in spiking networks. *Nature neuroscience*. 2009; 12:483–491. DOI: 10.1038/nn.2276 [PubMed: 19305402]
35. Rudy B, Fishell G, Lee S, Hjerling-Leffler J. Three groups of interneurons account for nearly 100% of neocortical GABAergic neurons. *Developmental neurobiology*. 2011; 71:45–61. DOI: 10.1002/dneu.20853 [PubMed: 21154909]
36. Kepecs A, Fishell G. Interneuron cell types are fit to function. *Nature*. 2014; 505:318–326. DOI: 10.1038/nature12983 [PubMed: 24429630]
37. Xue M, Atallah BV, Scanziani M. Equalizing excitation-inhibition ratios across visual cortical neurons. *Nature*. 2014; 511:596–600. DOI: 10.1038/nature13321 [PubMed: 25043046]
38. Xiang Z, Huguenard JR, Prince DA. Cholinergic switching within neocortical inhibitory networks. *Science*. 1998; 281:985–988. [PubMed: 9703513]
39. Hasselmo ME, Bower JM. Acetylcholine and memory. *Trends in neurosciences*. 1993; 16:218–222. [PubMed: 7688162]
40. Kruglikov I, Rudy B. Perisomatic GABA release and thalamocortical integration onto neocortical excitatory cells are regulated by neuromodulators. *Neuron*. 2008; 58:911–924. DOI: 10.1016/j.neuron.2008.04.024 [PubMed: 18579081]
41. Froemke RC, et al. Long-term modification of cortical synapses improves sensory perception. *Nature neuroscience*. 2013; 16:79–88. DOI: 10.1038/nn.3274 [PubMed: 23178974]
42. Dorn AL, Yuan K, Barker AJ, Schreiner CE, Froemke RC. Developmental sensory experience balances cortical excitation and inhibition. *Nature*. 2010; 465:932–936. DOI: 10.1038/nature09119 [PubMed: 20559387]
43. Metherate R, Weinberger NM. Cholinergic modulation of responses to single tones produces tone-specific receptive field alterations in cat auditory cortex. *Synapse*. 1990; 6:133–145. DOI: 10.1002/syn.890060204 [PubMed: 2237776]
44. Pinto L, et al. Fast modulation of visual perception by basal forebrain cholinergic neurons. *Nature neuroscience*. 2013; 16:1857–1863. DOI: 10.1038/nn.3552 [PubMed: 24162654]

45. Lin SC, Nicolelis MA. Neuronal ensemble bursting in the basal forebrain encodes salience irrespective of valence. *Neuron*. 2008; 59:138–149. DOI: 10.1016/j.neuron.2008.04.031 [PubMed: 18614035]
46. Schneider DM, Nelson A, Mooney R. A synaptic and circuit basis for corollary discharge in the auditory cortex. *Nature*. 2014; 513:189–194. DOI: 10.1038/nature13724 [PubMed: 25162524]
47. Lee S, Kruglikov I, Huang ZJ, Fishell G, Rudy B. A disinhibitory circuit mediates motor integration in the somatosensory cortex. *Nature neuroscience*. 2013; 16:1662–1670. DOI: 10.1038/nn.3544 [PubMed: 24097044]
48. Mayse JD, Nelson GM, Avila I, Gallagher M, Lin SC. Basal forebrain neuronal inhibition enables rapid behavioral stopping. *Nature neuroscience*. 2015
49. Kawai H, Lazar R, Metherate R. Nicotinic control of axon excitability regulates thalamocortical transmission. *Nature neuroscience*. 2007; 10:1168–1175. DOI: 10.1038/nn1956 [PubMed: 17704774]
50. Goard M, Dan Y. Basal forebrain activation enhances cortical coding of natural scenes. *Nature neuroscience*. 2009; 12:1444–1449. DOI: 10.1038/nn.2402 [PubMed: 19801988]
51. Huber D, et al. Multiple dynamic representations in the motor cortex during sensorimotor learning. *Nature*. 2012; 484:473–478. DOI: 10.1038/nature11039 [PubMed: 22538608]
52. Chen JL, Pfaffli OA, Voigt FF, Margolis DJ, Helmchen F. Online correction of licking-induced brain motion during two-photon imaging with a tunable lens. *The Journal of physiology*. 2013; 591:4689–4698. DOI: 10.1113/jphysiol.2013.259804 [PubMed: 23940380]
53. Vogelstein JT, et al. Fast nonnegative deconvolution for spike train inference from population calcium imaging. *Journal of neurophysiology*. 2010; 104:3691–3704. DOI: 10.1152/jn.01073.2009 [PubMed: 20554834]
54. Vallentin D, Kosche G, Lipkind D, Long MA. Neural circuits. Inhibition protects acquired song segments during vocal learning in zebra finches. *Science*. 2016; 351:267–271. DOI: 10.1126/science.aad3023 [PubMed: 26816377]

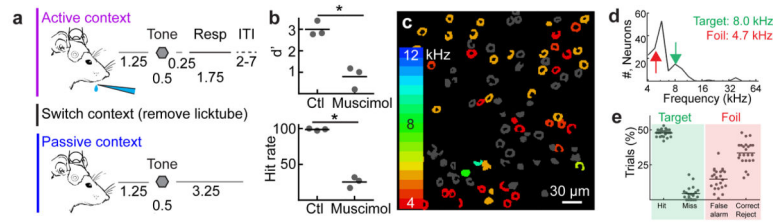


Figure 1.

Task design and auditory cue selection. **a**, Behavioral schematic showing trial structure. In the active context, pure tones are played for 0.5 s at 70 db SPL, followed by a 0.25 s grace period, and a 1.75 s response window. The inter-trial interval (ITI) varied based on behavioral outcome with false alarms eliciting a 4 s time-out. In the passive context, the target and foil tones were played in a pseudo-random sequence with other pure tones (500 ms, 70 db SPL). There was no punishment for licking in the passive context (i.e., the absence of licking was completely voluntary). **b**, Schematic of bilateral muscimol inactivation (1 μ l of 1 mg/ml). Muscimol inactivation severely impaired behavioral performance ($d' = 3.0 \pm 0.2$, muscimol $d' = 0.8 \pm 0.3$, mean \pm s.e.m., $n = 3$ animals, Student's paired two-tailed t-test, $t(2) = 7.733$, $p = 0.0163$; hit rate = 98.7 ± 0.9 , muscimol hit rate = $25.3 \pm 4.4\%$, mean \pm s.e.m., $n = 3$ animals, Student's paired two-tailed t-test, $t(2) = 20.79$, $p = 0.0023$). **c**, Example field-of-view for 2-photon Ca^{2+} imaging of tone-evoked activity in A1 of an awake mouse. Color indicates best frequency of each neuron. Gray, neurons that did not significantly respond to any tones played for baseline mapping between 4–64 khz. Note consistent low-frequency tuning in this field-of-view. **d**, Best frequency histogram (number of neurons with a certain best frequency). For this animal, the target was chosen to be 8 khz (green arrow) and the foil chosen to be 4.7 khz (red arrow). **e**, Summary of behavioral performance in 23 trained mice (hits: $47.2 \pm 0.9\%$, misses: $4.2 \pm 0.9\%$, false alarms: $15.2 \pm 1.7\%$, correct rejects: $33.9 \pm 1.6\%$; mean \pm s.e.m.).

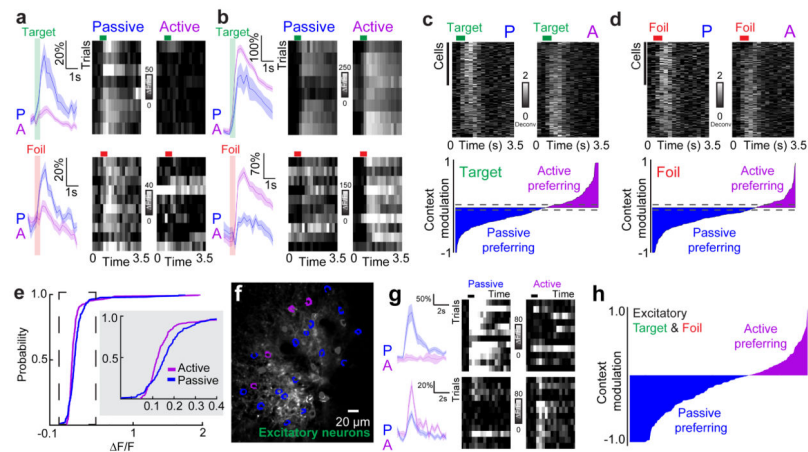
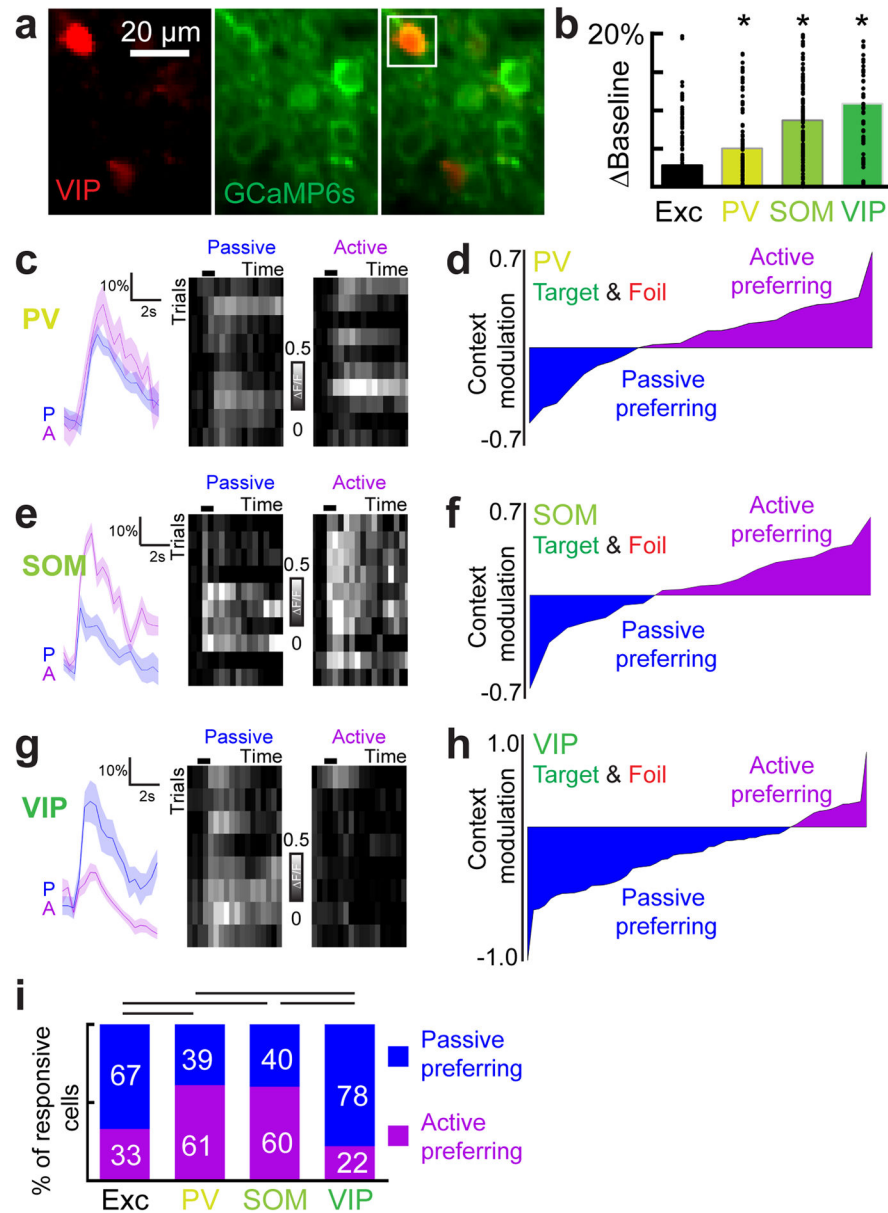


Figure 2.

Task engagement elicits suppression and facilitation of A1 neurons. **a**, Two example neurons (top, target tone responsive, $F/F=38\pm6\%$, passive, $11\pm2\%$, active; bottom, foil tone responsive, $F/F=29\pm3\%$, passive, $14\pm2\%$, active, mean \pm s.e.m.) from the same mouse showing suppression in the active context (left, traces and shading indicate mean \pm s.e.m.; right, 10 trial heatmap showing only correct trials, which include hits and correct rejects). Green and red horizontal bars indicate time of target or foil tone presentation, respectively. **b**, Two example neurons showing elevated tone-evoked responses in the active context (top, target tone responsive, $F/F=156\pm13\%$, passive, $200\pm2\%$, active; bottom, foil tone responsive, $F/F=40\pm4\%$, passive, $96\pm3\%$, active, mean \pm s.e.m.) in the active context (left, mean \pm s.e.m.; right, 10 correct trials). **c**, Putative spiking activity from deconvolved calcium signals of all target-responsive neurons, correct trials only in active context. Top, cells ($n=227$ from 5 animals) sorted from most suppressed to most activated when the context was switched from passive ('P') to active ('A'). Bottom, modulation index for target-responsive neurons. Dashed lines indicate the 95% confidence intervals of a shuffled distribution. **d**, Deconvolved spiking activity for foil-responsive neurons, correct trials only in active context. Top, cells ($n=210$ from 5 animals) sorted from most suppressed to most activated in the active context. Bottom, modulation index for foil-responsive neurons. Dashed lines indicate the 95% confidence intervals of a shuffled distribution. **e**, Cumulative distribution of mean tone-evoked responses for the active and passive contexts ($n=227$ cells, $p=0.0009$, Kolmogorov-Smirnov test). **f**, Example images of GCaMP6s (green) expressed specifically in excitatory neurons. **g**, Example of passive-context preferring excitatory neuron (top) and an active-context preferring neuron (bottom). **h**, Context modulation for all tone-responsive excitatory neurons ($n=142$ cells from 5 animals, correct trials only).

**Figure 3.**

Contextual modulation of inhibitory neurons. **a**, Example images of GCaMP6s (green) expressed in VIP+ interneurons. **b**, Comparison of trial-by-trial baseline calcium signal modulation across cell types (n=144 excitatory neurons, n=94 PV+ neurons, n=159 SOM+ neurons, n=79 VIP+ neurons, one-way ANOVA, $F(3,472)=14.97$, $p<0.0001$; $p<0.05$ in comparison to excitatory neurons for all cell types (*), Tukey's post-hoc test). Baseline levels were computed as the non-evoked calcium levels either before or after tone-evoked responses. **c**, Example of increased activity in PV+ interneuron during the active context, correct trials only. **d**, Modulation index for all tone-responsive PV+ interneurons (n=31 cells, correct trials only, $p=0.0065$, Fisher's Exact Test). **e**, Example of increased activity in SOM+ interneuron during the active context, correct trials only. **f**, Modulation index for all tone-

responsive SOM+ interneurons (n=20 cells, correct trials only, p=0.0335, Fisher's Exact Test). **g**, Example of decreased activity in VIP+ interneuron during the active context. **h**, Modulation index for all tone-responsive VIP+ interneurons (n=36 neurons, correct trials only, p=0.0407, Fisher's Exact Test). **i**, Comparison of context preference for each neuronal subtype (p<0.05 for excitatory pool (n=437 neurons) versus PV+ and SOM+, PV+ versus VIP+, and SOM+ versus VIP+, Kruskal-Wallis test with Dunn's post-hoc test).

Author Manuscript

Author Manuscript

Author Manuscript

Author Manuscript

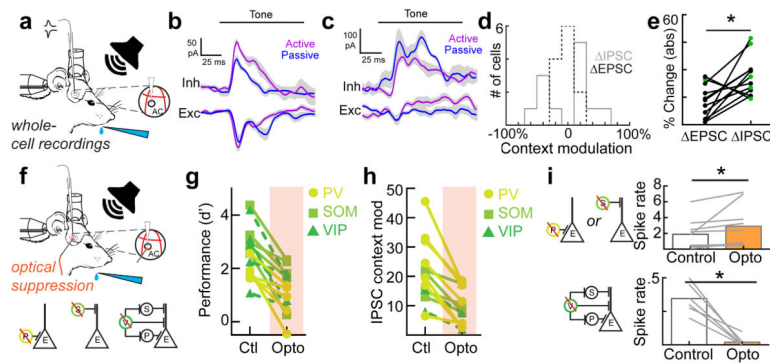


Figure 4.

Inhibition acts as a synaptic switch when changing contexts. **a**, Schematic of whole-cell recording experiments during behavior with exposed hole in cranial window for electrode access. **b**, An example cell showing greater change in inhibitory peak (34.9%) than excitation peak (9.4%) when switching contexts. **c**, An example cell showing a large change in inhibition (40.0%,) compared to excitation (15.5) when switching contexts. **d**, Histograms of changes in inhibition and excitation for all neurons ($n=12$ neurons, $n=4$ mice). **e**, Magnitude (absolute value) of inhibitory and excitatory changes in active versus passive contexts for all neurons (IPSC: $34.9 \pm 4.1\%$, EPSC: $16.1 \pm 3.5\%$, mean \pm s.e.m., $n=12$ cells, Student's paired two-tailed t-test, $t(11)=3.242$, $p=0.0079$ (*); green circles denote significant context-dependent changes in currents within neuron, $p<0.05$, Student's paired two-tailed t-test. **f**, Schematic of whole-cell recording experiments during behavior and optogenetic illumination. Circuit diagrams indicating inactivation of each interneuron subtype in separate experiments (optical suppression begins 100 ms before tone onset and continues for 100 ms after tone offset). **g**, Behavioral performance with and without optical suppression of PV, SOM or VIP interneurons (all: $n=15$ animals, control $d' = 2.6 \pm 0.2$, opto $d' = 1.1 \pm 0.2$, Student's paired two-tailed t-test, $t(14)=6.999$, $p<0.0001$; 'PV': $n=5$ animals, control $d' = 1.9 \pm 0.2$, opto $d' = 0.7 \pm 0.3$, Student's paired two-tailed t-test, $t(4)=3.5736$, $p=0.0233$; 'SOM': $n=5$ animals, control $d' = 3.2 \pm 0.3$, opto $d' = 1.7 \pm 0.4$, Student's paired two-tailed t-test, $t(4)=5.3464$, $p=0.0059$; 'VIP': $n=5$ animals, control $d' = 2.7 \pm 0.5$, opto $d' = 1.1 \pm 0.3$, Student's paired two-tailed t-test, $t(4)=3.3833$, $p=0.0277$. **h**, Summary of whole-cell voltage clamp recordings (all: $n=13$ neurons in 8 mice, IPSC(control): $42.0 \pm 6.0\%$, IPSC(opto): $19.6 \pm 3.5\%$, Student's paired two-tailed t-test, $t(12)=5.764$, $p<0.0001$; 'PV+': $n=7$ neurons in 3 mice, IPSC(control): $50.8 \pm 9.7\%$, IPSC(opto): $21.1 \pm 5.6\%$, Student's paired two-tailed t-test, $t(6)=5.350$, $p=0.0017$; 'SOM+': $n=5$ neurons, IPSC(control): $30.7 \pm 6.1\%$, IPSC(opto): $23.6 \pm 3.7\%$, Student's paired two-tailed t-test, $t(4)=3.109$, $p=0.0529$; VIP: $n=2$ neurons, IPSC(control): $23.5 \pm 7.5\%$, IPSC(opto): $9.3 \pm 5.4\%$, Student's paired two-tailed t-test, $t(1)=7.003$, $p=0.0903$). **i**, top; Optical suppression of PV+ or SOM+ interneurons increases pyramidal spiking in the active context (control= 1.9 ± 0.6 spikes per bin, opto= 2.9 ± 0.9 spikes per bin, Wilcoxon signed-rank test, $p=0.0039$, $n=5$ neurons with SOM+ inactivation (Wilcoxon signed-rank test, $p=0.0039$), and 4 neurons with PV+ inactivation (Wilcoxon signed-rank test, $p=0.0313$)). bottom; Optical suppression of VIP+ interneurons reduces pyramidal spiking in the active context (control= 0.34 ± 0.05 spikes per bin, opto= 0.02 ± 0.02 spikes per bin, Wilcoxon signed-rank test, $p=0.0313$, $n=6$ neurons).

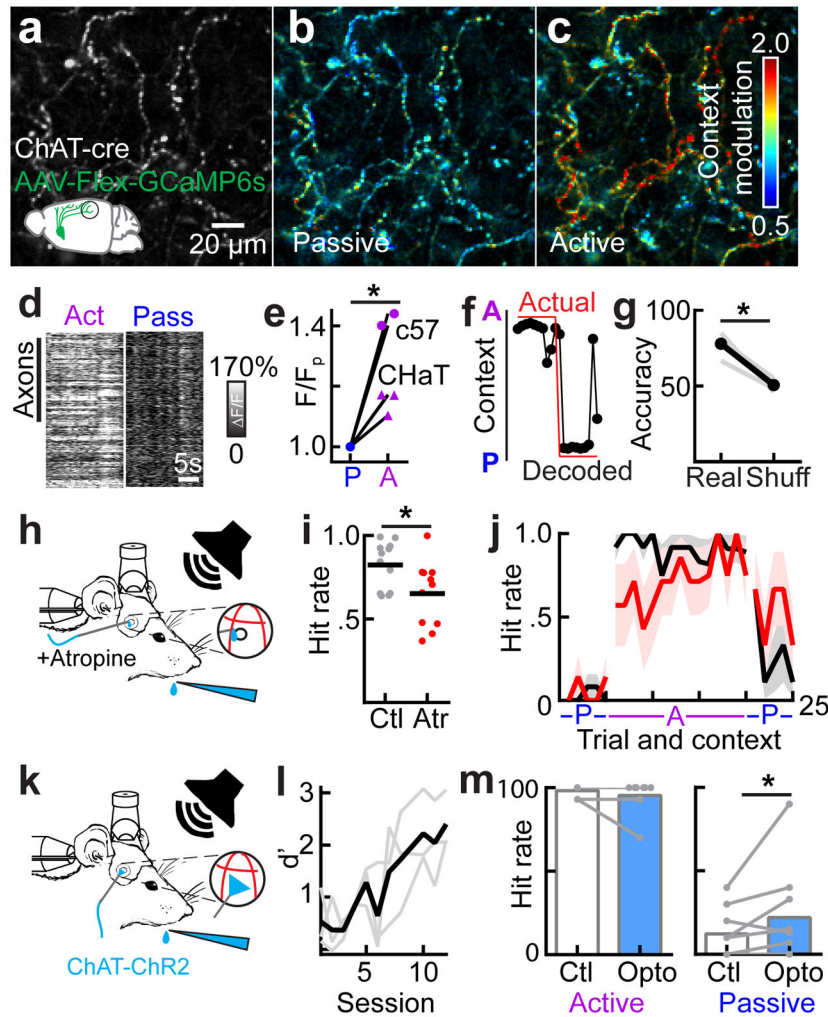


Figure 5. Cholinergic activity is necessary and partially sufficient to control behavior via inhibitory networks. **a**, Grayscale image of cholinergic axon segments in a *ChAT-cre* mouse. **b**, Image from **a**, pseudocolored to show differences in activity between two adjacent epochs of passive context behavior. **c**, Image from **a** pseudocolored to compare differences in average activity between two adjacent epochs (switching from active to passive). **d**, Axonal segments from one mouse. Each row represents the responses of one axon segment, where the grayscale indicates F/F across contexts ($n=333$ axon segments). **e**, Comparison of overall activity levels in the active versus passive context across animals (*ChAT-cre*: $n=3$ mice, $n=542$ cholinergic axon segments, $p<0.0001$ intra-animal, Student's paired two-tailed t-test; inter-animal, Student's paired two-tailed t-test, $t(2)=7.321$, $p=0.0181$; c57: $n=2$ mice, $n=1,058$ axon segments, $p<0.0001$ intra-animal, Student's paired two-tailed t-test). **f**, Performance of a Bayesian decoder on the axons shown in **a–c**. Red line denotes actual position of licktube and the associated behavioral context and the black circles and line indicates the decoded licktube position based solely on the cholinergic signal. **g**, Summary of decoding performance across animals and sites (Predicted: $77.9\pm 3.9\%$, Shuffled: $50.6\pm 2.0\%$, $n=4$ sites in 3 animals, Student's paired two-tailed t-test, $t(3)=6.394$, $p=0.0077$).

h, Behavioral schematic showing local unilateral application of atropine during behavior. **i**, Hit rate for unilateral application over auditory cortex (atropine hit rate: 0.65 ± 0.06 in 11 sessions, saline hit rate: 0.82 ± 0.04 in 12 sessions, Student's unpaired two-tailed t-test, $t(21)=2.439$, $p=0.0237$, $n=12$ control sessions; $n=11$ sessions with unilateral application of atropine to auditory cortex). **j**, In control conditions, when transitioning to the active context, the hit rate immediately reached steady state (first trial hit rate = $92 \pm 8\%$, steady state = $90 \pm 1.8\%$, $p=0.85$, Wilcoxon sign-rank test when comparing hit rate for trials 1–4 in the active context versus trials 11–14). In atropine conditions, the animal's hit rate started significantly lower before reaching steady state (first trial hit rate = $57.1 \pm 20.2\%$, steady state = $80.6 \pm 4.0\%$, $p=0.03$, Wilcoxon sign-rank test when comparing hit rate for trials 1–4 in the active context versus trials 11–14). **k**, Behavioral schematic showing optical illumination of auditory cortex during behavior. **l**, ChAT-ChR2 animals can learn the active context behavioral task within the same time frame as other genotypes ($n=3$ mice, trained $d' = 3.1 \pm 0.5$). **m, left**, The hit rate in the active context is not affected by optical activation of cholinergic terminals ($n=8$ sessions in 3 mice, $p=0.2188$, Wilcoxon signed rank test). **right**, The hit rate is significantly elevated by ~80% in the passive context during optical activation of cholinergic terminals (control: $12 \pm 5\%$, opto: $22 \pm 10\%$, $n=9$ sessions in 3 mice, $p=0.0156$, Wilcoxon signed rank test).

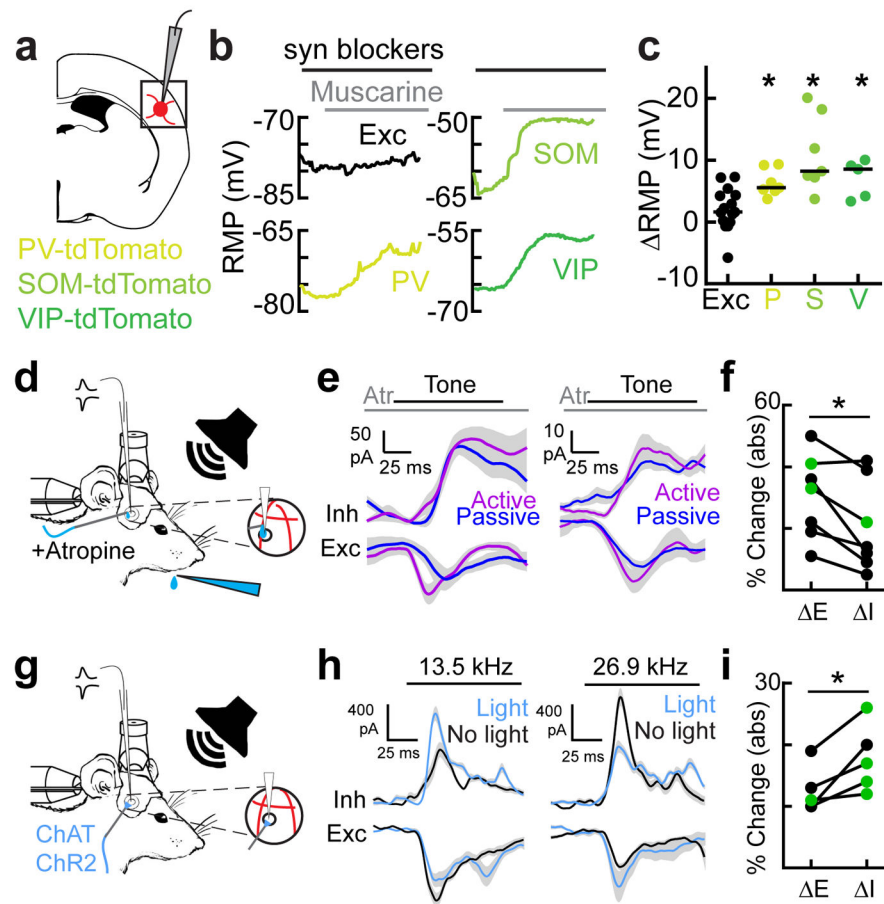
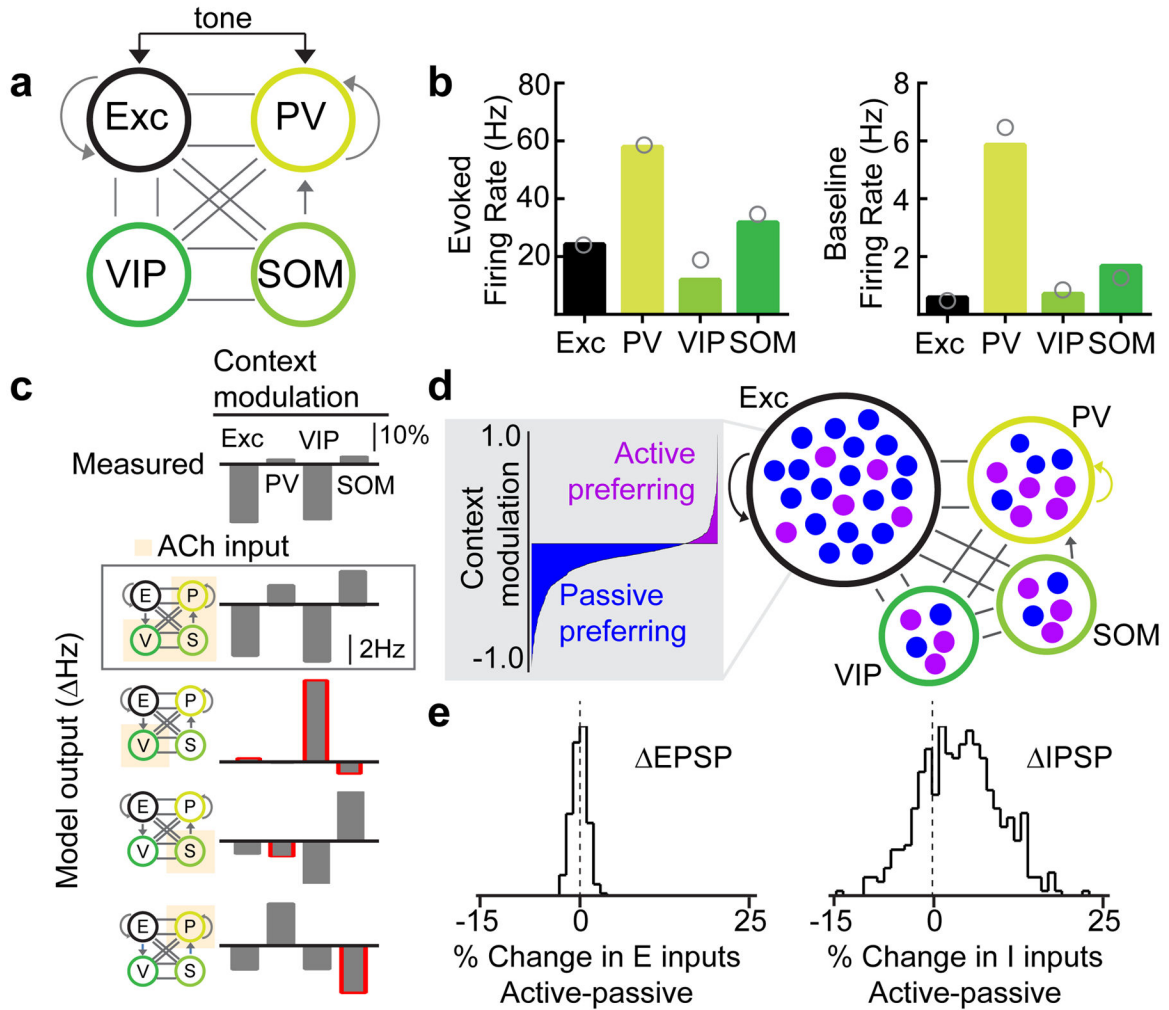


Figure 6.

Cholinergic activity impacts inhibition directly. **a**, Schematic of slice recordings in mice expressing tdTomato in either PV, SOM, or VIP interneurons. **b**, Example *in vitro* recordings from adult mouse auditory cortex showing average resting membrane potential (RMP) in 2s and 10s sweeps. Please note that spikes have been removed in the SOM+ recordings. Synaptic blockers (DNQX, APV and Picrotoxin) were washed in for at least 5 minutes prior to muscarine wash-in (1–2 μ M). **c**, Summary of *in vitro* recordings showing significantly greater depolarization of cortical interneurons in comparison to excitatory neurons (*overall*: $n=19$ interneurons, $n=15$ excitatory neurons, Student's unpaired two-tailed t-test, $t(32)=4.44$, $p=0.0001$, spikes removed; *cell-type specific responses*: PV+: $n=7$, median= $+5.6$ mV, interquartile range: 5.1–9.4; SOM+: $n=7$, median= $+8.2$ mV, interquartile range: 7.2–18.3; VIP+: $n=5$, median= $+8.6$ mV, interquartile range: 3.8–9.6; one-way ANOVA, $F(4,30)=9.015$, $p=0.0001$; $p<0.05$ for all interneuron subtypes versus excitatory neurons (PV: $p=0.0218$; SOM: $p<0.0001$; VIP: $p=0.0182$), Tukey's post-hoc test). **d**, Setup for whole-cell recording with local pharmacology in behaving head-fixed mice. **e**, Two example cells from two different animals that showed only modest contextual changes in tone-evoked IPSCs in presence of atropine (1 mM). **f**, Absolute value of change in inhibition versus excitation in atropine (IPSC: $19.7\pm 5.6\%$, EPSC: $30.3\pm 5.6\%$, $n=7$ cells, Student's paired two-tailed t-test, $t(6)=3.3252$, $p=0.0159$, green circles denote significant context-dependent changes in currents within neuron, $p<0.05$, Student's paired two-tailed t-test within neuron). **g**, Setup

for whole-cell recording and optogenetics in *Chat-ChR2* mice. **h**, Example recordings from the same cell, showing tone-evoked responses to 13.5 kHz (left) and 26.9 kHz (right) with and without optogenetic cholinergic modulation in auditory cortex. Left, 13.5 kHz responses showed greater increase in inhibitory peak (+38.8%) and integral (+23.4%) than decrease in excitatory peak (-35.9%) and integral (+0.0%). Right, 26.9 kHz responses showed greater decrease in inhibitory peak (-85.2%) and integral (-30.0%) than increase in excitatory peak (+35.6%) and integral (+24.3%) when switching optogenetic illumination on and off. **i**, Magnitude (absolute value) of inhibitory and excitatory changes between optogenetic illumination on and off for all neurons across complete tuning curve (IPSC: $17.8 \pm 2.5\%$, EPSC: $12.6 \pm 1.7\%$, $n=5$ cells, Student's paired two-tailed t-test, $t(4)=3.399$, $p=0.0273$, green circles denote significant context-dependent changes in currents within neuron, $p < 0.05$, Student's paired two-tailed t-test within neuron).

**Figure 7.**

Network model demonstrates requirement for co-activation of inhibitory and disinhibitory circuit elements. **a**, Schematic of the four-unit rate-based model. **b**, Evoked and baseline firing rates of each cell type in the 4-unit model. Gray circles represent experimental values derived from the literature. **c**, Changes in activity of all subtypes due to context (Active – Passive). The top plot shows the experimental values in terms contextual modulation index. The remaining plots relate to the network model and show changes in firing rates when acetylcholine activates PV+, VIP+, & SOM+ populations either simultaneously (second plot) or individually (third through fifth plots). Red outlines indicate directional changes that do not match the observed direction of change. **d**, Schematic of the multi-unit model in which each population is comprised of several rate units. The gray box shows the distribution of active and passive preferring excitatory cells in the model. **e**, Histograms of the changes in synaptic inputs due to context (in terms of percent of total input in passive condition) for total excitatory (left) and inhibitory (right) input to individual E cells in the multi-unit model. Note the diversity in inhibitory inputs.